China Geology 8 (2025) 431−453

China Geology

Journal homepage: http://chinageology.cgs.cn
https://www.sciencedirect.com/journal/china-geology

Geology, mineralization and model of the giant Maoping carbonate-hosted Pb-Zn deposit (5 Mt), South China

Ye He[a, b], Bang-Tao Sun[c], Hai-Peng Wang[a], Jia-Xi Zhou[a, b,*], Yan-Jun Li[d], Foteini Drakou[e], Kai Luo[a, b], Saleh Ibrahim Bute[a, b]

[a] *Key Laboratory of Critical Minerals Metallogeny in Universities of Yunnan Province, School of Earth Sciences, Yunnan University, Kunming* 650500, *China*
[b] *Yunnan International Joint Laboratory of China-Laos-Bangladesh-Myanmar Natural Resources Remote Sensing Monitoring, Kunming* 650500, *China*
[c] *Yiliang Chihong Mining Co. Ltd., Zhaotong* 657600, *China*
[d] *School of Earth Resources, China University of Geosciences, Wuhan* 430074, *China*
[e] *Department of Geology, Trinity College Dublin, Dublin* 2, *Ireland*

ARTICLE INFO

Article history:
Received 27 August 2024
Received in revised form 6 December 2024
Accepted 26 December 2024
Available online 21 January 2025

Keywords:
Ore deposit geology
Mineralogy
Geochemistry
Geochronology
Ore deposit formation and evolution
Ore-forming model
Maoping carbonate-hosted Pb-Zn deposit
SW China

ABSTRACT

The giant Upper Yangtze Pb-Zn metallogenic province, also known as the Sichuan-Yunnan-Guizhou (SYG) Pb-Zn province hosting >500 carbonate-hosted epigenetic Pb-Zn deposits that contain >20 Mt Pb + Zn base metal reserves. The giant Maoping Pb-Zn deposit is the second largest deposit in this province and owns >5 Mt Pb + Zn metal reserves with ore grades of 12 wt.%-30 wt.% Pb + Zn. Such large tonnages and high grades make it among the top 100 similar mineral deposits in the world. The ore bodies are predominantly located within the strata of the Upper Devonian (Zaige Formation) and Lower (Baizuo Formation)-Upper (Weining Formation) Carboniferous. The principal ore minerals consist of galena (Gn), sphalerite (Sp), and pyrite (Py), while the primary gangue minerals include dolomite (Dol), calcite (Cal), and quartz (Qtz). Three mineralization stages of carbonate minerals have been identified: (1) pre-sulfide stage 1, (2) syn-sulfide stage 2, and (3) post-sulfide stage 3. Trace elements and C-O-Sr isotopes of three stages' carbonate minerals, together with S-Pb isotopes of sulfides, revealing that the metamorphic basement rocks played the role of the metal source during the early stage of Pb-Zn mineralization, whereas the metal contribution of the sedimentary wall rocks found to be more prominent during the late stage of Pb-Zn mineralization. In addition, the dissolution of marine carbonate rocks and CO_2 degassing may have also played an important role in the formation of the Maoping deposit. Furthermore, syn-sulfide stage 2 calcite has a U-Pb age of 214 ± 20 Ma obtained by LA-ICPMS in-situ analyses, suggesting that the hydrothermal mineralization occurred during the Triassic. Our study proposes a new coupled metallogenic model of fluid-structure-lithology assemblage and provides new insights about the formation and evolution of the Maoping deposit with significant implication for understanding and exploration of similar Pb-Zn deposits worldwide.

1. Introduction

The giant Maoping carbonate-hosted Pb-Zn deposit is in the southwestern margin of the Yangtze Block, South China and is the second-largest (5 Mt) deposit in the Upper Yangtze (also known as Sichuan-Yunnan-Guizhou, SYG) Pb-Zn metallogenic province. The Upper Yangtze province is the most concentrated metallogenic zone/belt for epigenetic Pb-Zn deposits that contain at least 20 Mt Pb + Zn base metal reserves in China and is also one of the most important Pb-Zn metallogenic zones/belts in the world. The Maoping Pb-Zn deposit is currently one of the largest Pb-Zn deposits being mined in China, and is also the main mine of the Yiliang Chihong Co., Ltd. The mining capacity of this deposit is 600000 t of ores per year. For example, in 2016, the sales revenues were close to RMB 1.5 billion. Therefore, conducting systematic research on this deposit has important theoretical significance and economic value.

Previous studies focused primarily on sulfide minerals and have provided significant insights into the ore genesis (Zhang

First author: *E-mail address*: 251208570@qq.com (Ye He).

* Corresponding author: *E-mail address*: zhoujiaxi@ynu.edu.cn (Jia-Xi Zhou).

Literary editor: Xi-jie Chen
doi:10.31035/cg2024142
2096-5192/© 2025 China Geology Editorial Office.

CQ et al., 2005; Xiang ZZ et al., 2020). However, there is no consensus about the timing of mineralization with variable isotope ages to have been reported in the literature, ranging from 201 Ma to 448 Ma (Shen ZW et al., 2016; Yang B et al., 2018, Yang Q et al., 2018).

Hydrothermal carbonate minerals, such as calcite and dolomite, are the most abundant gangue minerals in carbonate-hosted Pb-Zn deposits, and their experiencing the entire mineralization process, recording valuable information about the mineralization and offering important insights for a more robust understanding of hydrothermal mineralization (Zhou JX et al., 2013a, 2013b, 2013c, 2018a). On the other hand, determining ages of carbonate-hosted epigenetic Pb-Zn sulfide deposits are difficult due to the lack of suitable minerals and methods (Leach DL et al., 2005; Leach DL and Song YC, 2019). Previous attempts for dating such type of Pb-Zn deposits employed Rb-Sr isotopes of sphalerite and pyrite (Nakai S et al., 1993; Zhou JX et al., 2013d, 2015; Yang B et al., 2018; Yang Q et al., 2018; Yang Q, 2021), Sm-Nd isotopes of calcite and fluorite (Li WB et al., 2004b, 2007; Mao JW et al., 2012; Zhou JX et al., 2013d; Zhang CQ et al., 2015) and U-Th-Pb isotopes of calcite (Brannon JC et al., 1996). Although these methods have been successfully applied to date the carbonate-hosted epigenetic Pb-Zn deposits, there are limitations resulting them difficult to be apply uniformly. Carbonate minerals have been recently demonstrated to be suitable for U-Pb dating by in-situ laser ablation-inductively coupled plasma-mass spectrometry (LA-ICPMS) technique that allows for precise acquisition of trace elements and isotopes (Luo K et al., 2020a; Yang Q, 2021). *In-situ* U-Pb dating of carbonate minerals using LA-ICPMS has been applied to several hydrothermal deposits (Luo K et al., 2020a; Jin XY et al., 2021; Xiong SF et al., 2022).

In this paper, ore deposit geology, mineralogy, cathodoluminescence (CL), *in-situ* trace elements and Sr isotopes, bulk C-O isotopes and *in-situ* U-Pb ages of carbonate minerals, together with S-Pb isotopes of sulfides obtained by previous studies, provide the comprehensive information for understanding the source, ore-forming condition and process, and the timing of mineralization. Compared with other Pb-Zn deposits in the Upper Yangtze Pb-Zn metallogenic province, the multi-layer metallogenesis of the Maoping deposit is improved, and a complete metallogenic model is established, which provides a new perspective for the better understanding of the formation of the carbonate-hosted epigenetic Pb-Zn deposits and exploration efforts for similar Pb-Zn deposits worldwide.

2. Regional geological setting

The Upper Yangtze Pb-Zn metallogenic province is spatially associated with the Emeishan Large Igneous Province (ELIP), and is an important part of the low-temperature hydrothermal metallogenic domain in South China (Fig. 1a; Zhou MF et al., 2002). Structurally, this province is in the western margin of the Yangtze Block, and is adjacent to the Songpan-Ganzi Terrain in the north, the Sanjiang Orogenic Belt in the southwest, and the Cathaysian Block in the southeast (Fig. 1b). The triangular area is controlled by three major faults, including the NS-trending Anninghe - Lvzhijiang Fault, the NE-trending Mile - Shizong - Shuicheng Fault, and the NW-trending Kangding - Yiliang - Shuicheng Fault (Fig. 1a; Zhang CQ et al., 2005).

In the western Yangtze Block, the metamorphic basement complexes are unconformably overlaid by the sedimentary covers. Most scholars believe that the metamorphic basements include the lower crystalline basements and the upper fold basements. The fold basements consist of a set of clastic flysch construction, including medium to low-grade metamorphic rocks of the Meso-and Neo-Proterozoic Kunyang and Huili Groups; and the crystalline basements are mainly composed of high-grade metamorphic rocks such as gneiss and granitic migmatitic gneiss in the Paleo- and Meso-Proterozoic Kangding Group (Liu HC and Lin WD, 1999).

Marine cap is mainly composed of marine carbonates and continental sedimentary rocks (Table S1). The lower part is characterized by marine sedimentary rocks of Early Paleozoic to Middle Triassic, which consist of the Upper Ediacaran thick-layer dolomite, Cambrian interbedded black shale, sandstone, and dolomite, Ordovician to Devonian limestone, shale and sandstone, and Carboniferous limestone and dolomite. The Permian strata are dominated by carbonates and the Emeishan flood basalts (about 260 Ma), whereas the Triassic strata are composed of thin-bedded limestone and shale (Zhou MF et al., 2002). The upper part is comprised of Middle Jurassic to Quaternary continental sedimentary rocks, with local occurrences of feldspathic quartz sandstone, siltstone, mudstone, and coal seams (Zhou JX et al., 2013c). Evaporates and organic matters occur within the Devonian-Carboniferous sedimentary rocks (Zhou JX et al., 2018b). The basement rocks have experienced a period of protracted deformation and metamorphism during the Neoproterozoic. During the Hercynian (Late Paleozoic), the north-south deep faults developed due to the continuous east-west tension. A large-scale Emeishan basalts erupted along these deep faults (Huang ZL et al., 2004). During the Indosinian (Early Mesozoic), a series of NE-trending thrust-folded tectonic zones were formed in the NE Yunnan owing to the strong northward compression. This stage is considered the main period for the formation of Pb-Zn deposits in the Upper Yangtze province (Ma L et al., 2004). During the Yanshanian (Late Mesozoic), the north-south deep fractures showed a characteristic of compression due to the NNE-SSW compressive stress. Moreover, the Himalayan (Cenozoic) movement caused a strong compression event in the Upper Yangtze province (Fig. 1a).

The study area exposes a large amount of Emeishan basalts, which covers almost the entire Upper Yangtze Pb-Zn metallogenic province. The Emeishan basalts, situated in the southwestern part of China, to the east of the Red River-Ailao Shan suture zone, developed along the Panxi Rift axis. Structurally, the ELIP is delineated into three zones: the inner,

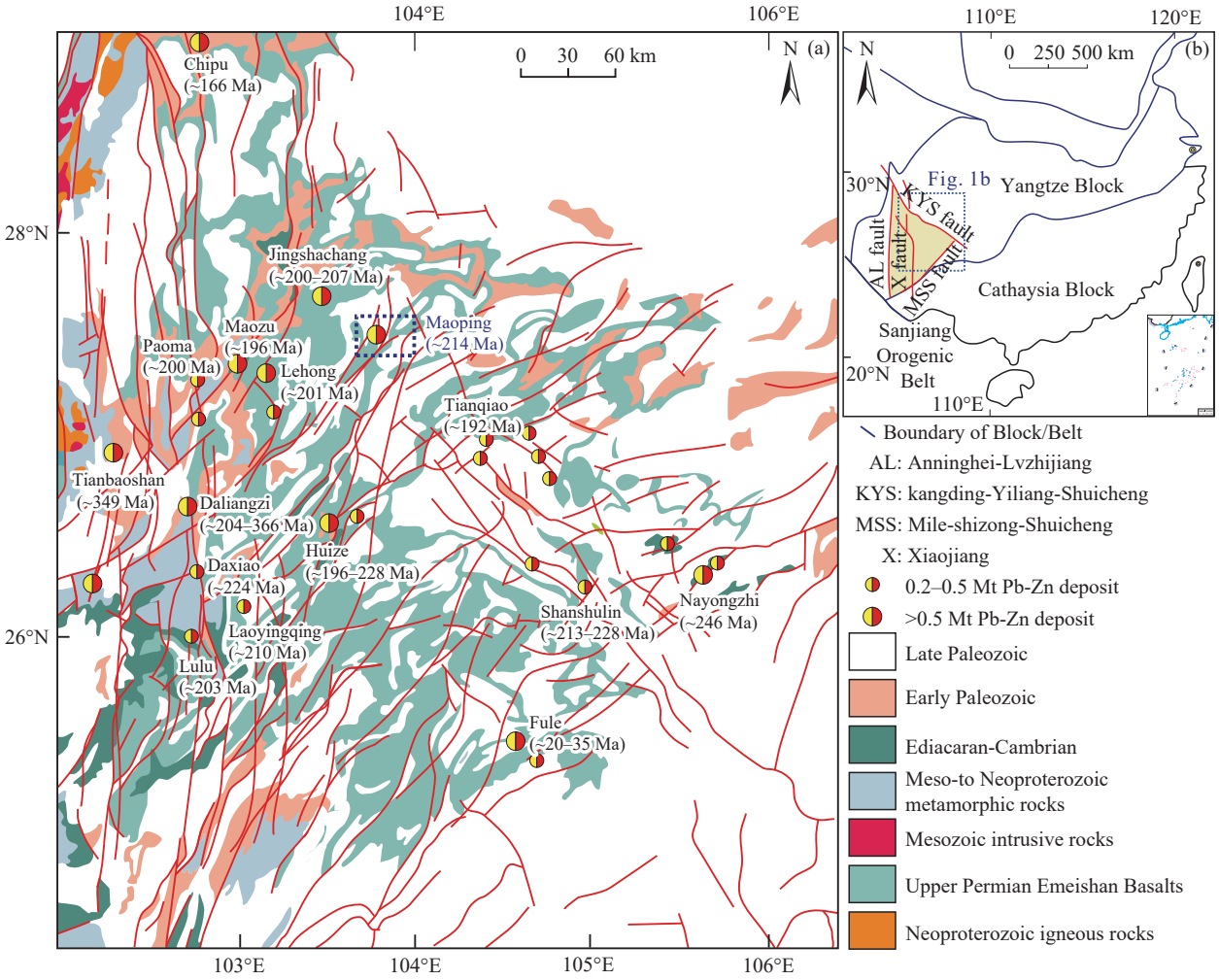

Fig. 1. (a) Geological map of the Upper Yangtze Pb-Zn metallogenic province (modified from Zhou JX et al., 2018b), and (b) Tectonic map of South China. Ages are from Huang ZL et al. (2004), Li WB et al (2004a, 2004b, 2007), Yin MD et al. (2009), Liu F (2005), Liu XK et al. (2022), Lin ZY et al. (2010), Mao JW et al. (2012), Wu Y (2013), Zhang CQ et al. (2008, 2014, 2015), Zhou JX et al. (2013a, 2013c, 2015), Liao KL et al. (2020), Guan HM et al. (2020), Wang J et al. (2019) and Gong HS et al. (2021).

middle, and outer zones, with the inner zone possessing the thickest crust and the outer zone being comparatively thinner (Shellnutt JG et al., 2020).

3. Geology of the mining area

The Maoping Pb-Zn deposit is in the eastern side of the NS-trending Xiaojiang Fault and is jointly controlled by the NW-trending Kangding-Yiliang-Shuicheng deep Fault and the Huize-Yiliang Fault (Fig. 1).

3.1. Strata

The main rocks distributed in the mining area are Silurian to Triassic sedimentary rocks, Upper Permian Emeishan basalts, and a small amount of Quaternary, with the absence of the Early Paleozoic and Precambrian. The Zaige Formation of Upper Devonian, Baizuo Formation of Lower Carboniferous, and Weining Formation of Upper Carboniferous are the main ore-bearing strata (Fig. 2; Li LR and Li DL, 2016), with the surrounding rocks mainly composed of dolomite. The third section of the Zaige Formation is divided into three sub-sections, with the main ore-bearing strata in the second sub-section, mainly consisting of thick layers of gray to gray-white dolomite, with the No. I ore body occurring in the middle. The lithology of the Baizuo Formation is mainly gray to pink thick dolomite, with lens-shaped Pb-Zn ore bodies in the upper part. The Weining Formation can be divided into two sections, with the first sub-section mainly composed of light gray dolomite and limestone, containing the No. II ore body in the middle, and the second sub-section mainly consisting of gray-white medium-thick limestone. The second sub-section lithology is light gray to gray-white medium-thick fine-grained limestone, with 1–2 m of green shale in the middle, and the No. II ore body occurring in the middle. The third sub-section lithology is gray medium-thick dolomite and limestone, with veined or lenticular Nos. III, HI, and SI ore bodies in the upper-middle part (Wei AY et al., 2015). The Liangshan Formation of Lower Permian is purple-red to beige sand shale; the Qixia-Maokou Formation of Middle Permian is mainly gray limestone; and the Emeishan Basalts Formation of Upper Permian consists of green dense blocky, almond-shaped, or

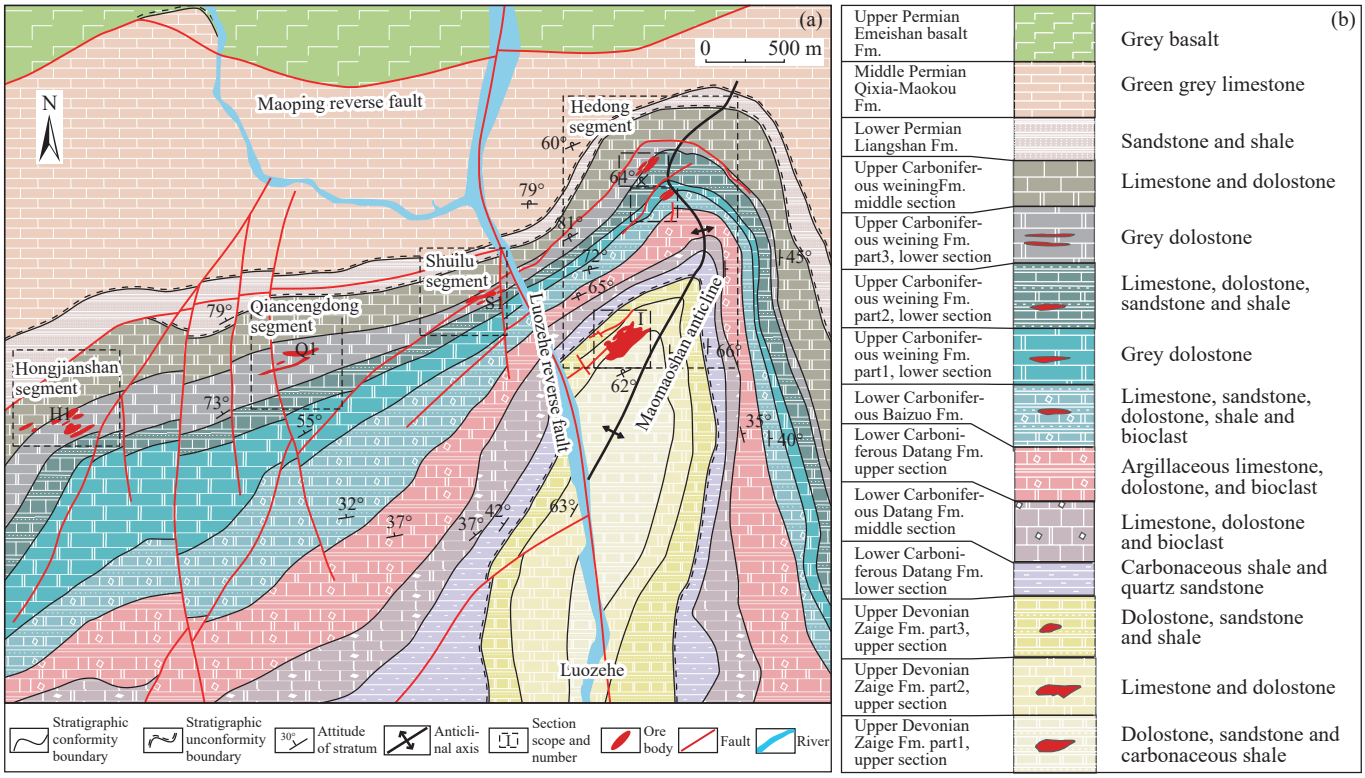

Fig. 2. a–Geological map of the Maoping area and b–Stratigraphic histogram map of the Maoping Pb-Zn deposit (modified from Wang L et al., 2022).

vesicular Emeishan basalts.

3.2. Structures

The left-lateral strike-slip tectonic stress of the Xiaojiang fault has resulted in a series of compressional-twist fold and fault structures in the mining area. The main structures in the area are the Maomaoshan overturned anticline, with a length of about 20 km, showing an overall inclined fold morphology, with many compressional-twist interlayer fractures developed near the axis. The strata at the axis are from the Upper Devonian, with asymmetric wings. The eastern wing has gently dipping strata with angles of 30°–40°, mainly consisting of Carboniferous and Permian limestone, dolomite, and mudstone; while the western wing has overturned nearly vertical distribution, with angles of 65°–90°, mainly composed of the Qixia-Maokou Formation, and the Datang and Weining Formations of Carboniferous (Figs. 2 and 3; Wei AY et al., 2015; Wang L et al., 2022).

The secondary structures in the mining area are characterized by the NE-SW and NW-SE trending fault systems. The NE-SW fault system includes the Maoping thrust fault and the Hedong fault group, while the NW-SE fault system mainly consists of the Luozehe fault and the Hexi fault group (Figs. 2 and 3). Specifically, (1) the Maoping thrust fault is lens-shaped and foliated, with a SE trend and a dip angle of 60°–85°, directly controlling the distribution of Pb-Zn ore bodies in the Maoping mining area, with the hanging wall forming the Huamiaozhai overturned anticline; (2) the Hedong fault group comprises small-scale faults, mostly interbedded faults trending along the stratigraphy in a SE direction with dip angles of 60°–85°, exhibiting characteristics of thrusting and overthrusting SE-NW; (3) the Luozehe fault extends along the Luoze River for over 800 m with a SW trend, disappearing near the confluence of the Luoze River in the northwest and transitioning to a northwest trend in the south after extending beyond the mining area; and (4) the Hexi fault group consists of small-scale faults, primarily strike-slip faults concentrated in the area from the Hexi, Shuolu and Hongjianshan mines.

4. Mineralization and alteration

4.1. Ore body characteristics

The Maoping Pb-Zn deposit manifests as concealed to semi-concealed ore bodies situated within the core and flanking regions of the Maomaoshan anticline. The distribution of these ore bodies generally aligns with the geological strata, extending in a northeast-southwest direction and inclined towards the southeast. The dip angles of the ore bodies predominantly range from 50° to 80°, exhibiting considerable vertical extension. Because the Luoze River runs through the verification area in a north-south direction, dividing the verification area into two parts: east of the river and west of the river.

The group of No. I ore bodies is located within the Upper Devonian Zaige Formation, presented in layered, lens-shaped, and vein-like configurations. The general strike of the ore bodies is usually between 30°–54°, with steeply dipping ore

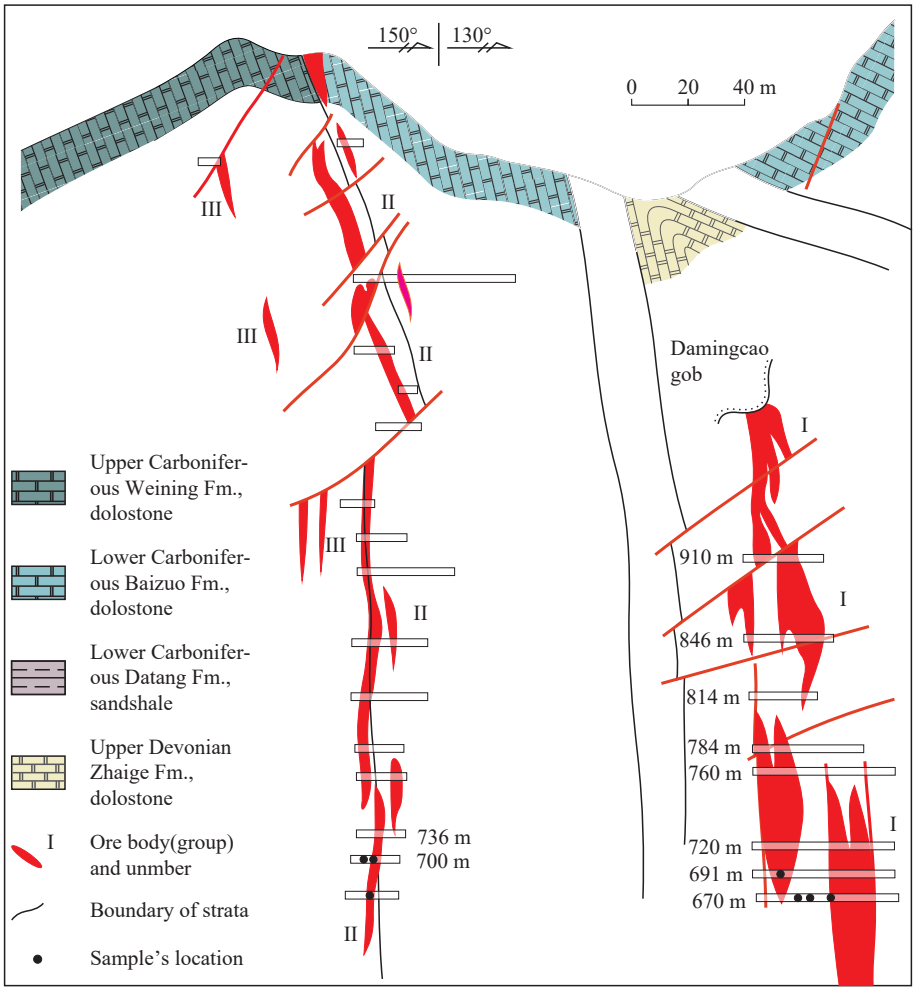

Fig. 3. Typical cross exploration map of the Maoping Pb-Zn deposit (modified from Wei AY et al., 2015).

bodies having an angle of dip typically ranging from 60° to 83°, locally nearly vertical; gently dipping ore bodies have an angle of dip generally between 46°–58°. The ore bodies are characterized by a small strike extension (the main ore bodies strike length is generally 230–300 m, and the minor ore bodies strike length is generally 20–60 m) and a large dip extension (the main ore bodies dip depth is generally about 400 m).

Located on the northwest flank of the Maomaoshan anticline, the ore bodies are hosted in the second member of the Upper Carboniferous Weining Formation. The ore bodies occurring in the first and second sub-members are classified as the group of No. II ore bodies, the group of No. III ore bodies occur in the third sub-members. The ore bodies occur as lenticular, and irregular shapes. The ore bodies generally trend between 50°–85°, the dip angle is usually between 70°–87°, and locally it is nearly vertical. The group of No. II ore bodies is characterized by a small strike extension (the main ore bodies typically have a strike length of about 140–170 m, while the minor ore bodies have a strike length of about 2–80 m) and a large dip extension (the main ore body generally dip to a depth of about 680 m). The group of No. III ore bodies also shows a small strike extension (the main ore bodies typically have a strike length of about 50–130 m, while the minor ore bodies have a strike length of about 4–60 m) and a large dip extension (the main ore bodies generally dip to a depth of about 240 m).

The newly-discovered group of No. VI ore bodies is in the southwestern direction of the group of No. I ore bodies, with multiple ore bodies discovered along the 98–82 exploration lines, and is controlled by 27 drill holes (Fig. 2; He Y et al., 2023). This ore bodies are of a large scale (> 0.6 Mt Pb + Zn metal reserves), occur within the first member of the Upper Devonian Zaige Formation and are surrounded by medium crystalline dolomite. Ore bodies in this group exhibit a relatively regular layered occurrence and trend in alignment with the geological strata. It is NE-SW trending, dipping southeast at an angle of 55°, with some areas showing a gentle dip. It extends approximately 320 m in length and 300 m in dip length, with thickness of 0.20–90.89 m (mean 16.62 m).

The group of the S1, Q1, H1, and Longxiang ore bodies are in the southwest extension of the group of Nos. II-III ore bodies, with the ore-hosting strata being the Upper Carboniferous Weining Formation. Th ore bodies occur in the second member, third sub-member of the Carboniferous Weining Formation, with a relatively small scale and often lens-shaped, layered-like, tubular, vein-like and a steeper dip angle.

The group of the S1 ore bodies generally trends between 55°–90°, and the dip angle usually between 80°–85°. The ore bodies are characterized by a small extension along the strike (the main ore bodies are generally about 97 m, and the minor ore bodies are about 29–81 m) and a small extension along the dip (the main ore bodies generally extend about 164m deep, and the minor ore bodies are about 64–210 m).

The group of the Q1 ore bodies generally trends between 60°–90°, and the dip angle usually between 70°–90°. The overall characteristics are of a small extension along the strike (the main ore bodies are generally about 40 m, while the minor ore bodies are usually between 6–40 m) and a small extension along the dip (the main ore bodies are generally about 98 m, and the minor ore bodies are usually between 4–50 m).

The group of the H1 ore bodies generally trends between 30°–80°, the dip angle usually between 70°–88°, and locally it is nearly vertical. The overall characteristics are of a small extension along the strike (the main ore bodies are generally about 78 m, while the minor ore bodies are usually between 10–130 m) and a large extension along the dip (the main ore bodies are generally about 410 m).

The group of the Longxiang ore bodies generally trends between 50°–90°, and the dip angle usually between 62°–73°. The overall characteristics are of a small extension along the strike (the main ore bodies are generally about 200 m, while the minor ore bodies are usually 80 m) and a small extension along the dip (the main ore bodies are generally about 150 m).

The group of the Xiushuigou ore bodies are located at the southwest extension end of the group of Nos. I and VI ore bodies, with the ore-hosting stratum being the second member of the Upper Devonian Zaige Formation. The ore bodies are lens-shaped, with a general strike of 30°–80°. The ore bodies trend northwest with a general dip angle of 52°–60°. The overall characteristics are of a small extension along the strike (the main ore bodies are generally about 115 m, while the minor ore bodies are usually 81 m) and a small extension along the dip (the main ore bodies are generally about 128 m).

The group of the Zuanbaoshan ore bodies are in the southwest extension end of the group of Xiushuigou ore bodies. The ore bodies are stratiform, layered and vein-like., with a general strike of 10°–50°. The ore bodies trend northwest with a general dip angle of 50°–70°. The overall characteristics are of a large extension along the strike (the main ore bodies are generally about 280 m, while the minor ore bodies are usually 90 m) and a small extension along the dip (the main ore bodies are generally about 60 m).

4.2. Characteristics of minerals

The symbiotic mineral assemblage in the Maoping Pb-Zn deposit is relatively simple, consisting mainly of metal sulfides such as galena (Gn), sphalerite (Sp), and pyrite (Py), and gangue minerals composed mainly of dolomite (Dol), calcite (Cal), and quartz (Qtz) (Table 1; Figs. 4-8). The ore and gangue minerals exhibit various textures, including idiomorphic-allomorphic granular (Fig. 7a, d, e, and g), inclusion (Fig. 7a), fractured (Fig. 6b), and co-border textures (Fig. 7f). The ore minerals show massive (Fig. 5c, e, and h), veined (Fig. 5b, e, f, and h) and disseminated structures (Fig. 5d), while gangue minerals mainly exhibit veined (Figs. 4a-b, 5f, and 6a, h, i), veinlet (Figs. 4d-f, 5b, f, h, 6a, c, e, and 7c, f), nodular (Figs. 4c-e, 5c, d, e, g, and 6b, e), and vug structures (Fig. 5a and i).

Table 1. Mineral formation sequence.

Minerals	Stage 1	Stage 2	Stage 3
Sphalerite		Sp-1	Sp-2
Galena		Gn-1	Gn-2
Pyrite	Py-1	Py-2	Py-3
Dolomite	Dol-1	Dol-2	Dol-3
Calcite	Cal-1	Cal-2	Cal-3
Quartz			

More Less

4.3. Alteration of surrounding rocks

Hydrothermal alteration in the Maoping deposit include pyritization, dolomitization, and calcitization. Hydrothermal dolomite occurred in the form of medium to coarse grained disseminated and as fine veins in the dolostone. Calcite is fine metacyst and occurs within dolostone blocks as disseminated grains and veins of different sizes, is also found along joints or fractures of dolostone in irregular veins. Pyrite is fine-grained and occurs within dolomite mostly as disseminated grains as well as in the form of veins. The silicification is weak and described by fine quartz found within dolomite or calcite in granular and agglomerated form (Zou HJ et al., 2004).

4.4. Mineralization stage and mineral assemblage

Based on macroscopic observations such as field geological survey and hand specimen, combined with microscopic observation using ordinary light microscopy, scanning electron microscopy, and Cathode Luminescence, detailed mineralogical studies were conducted. The hydrothermal rocks of the Maoping deposit can be divided into sulfides + carbonates and carbonates two types. Hence, the carbonate minerals can be further divided into pre-sulfide stage 1, syn-sulfide stage 2, and post-sulfide stage 3 three types (Table 1; Figs. 4-8).

During the stage 1, the mineral assemblage consists of Py-1, Dol-1, and Cal-1, with fine-grained Py-1 showing high degree of idiomorphism, distributed in a star-like pattern within the host rocks, with some growing along fractures to form veinlets (Fig. 6g). Dol/Cal-1 is reticular distributed in the host rocks, with some showing intergrowths with sulfides (Figs. 4b, 5e, 6a, h, i, 7b, and 8a). Carbonate minerals exhibit

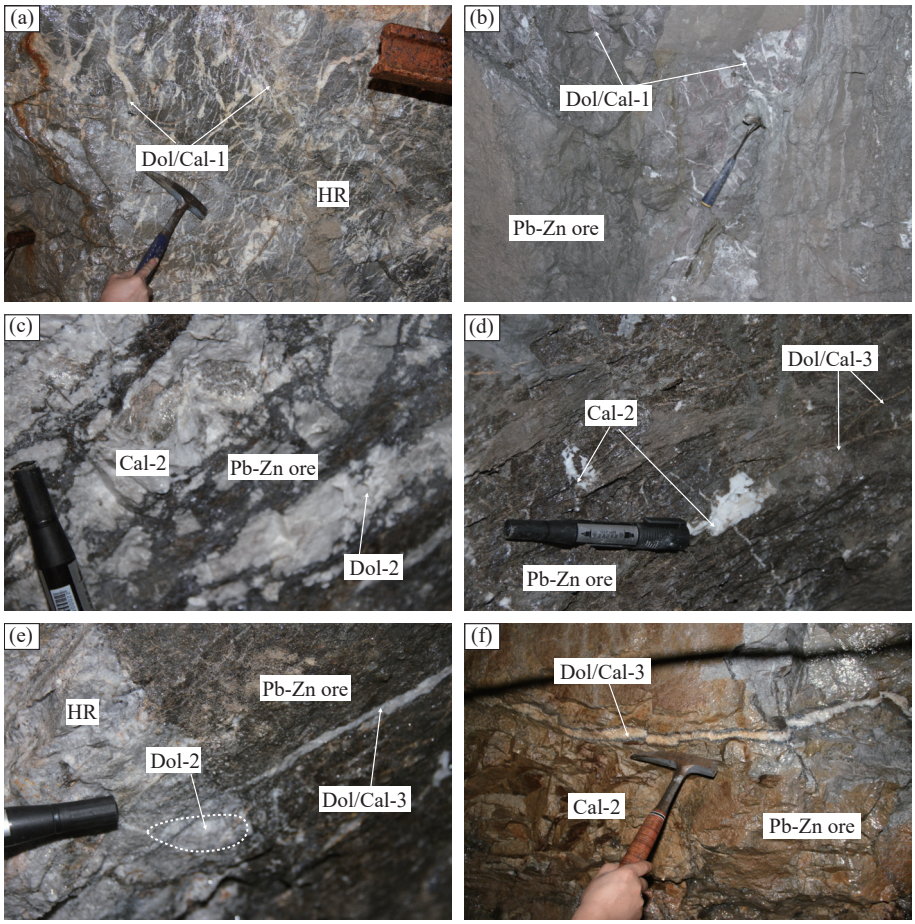

Fig. 4. Ore field photos of the Maoping Pb-Zn deposit. (a) Dol/Cal-1 veinlets in host-rocks; (b) Pb-Zn ores and Dol/Cal-1 veins interspersed by ore bodies; (c) Lumpy Dol/Cal-2 coexists with Pb-Zn ore bodies; (d), (f) Lumpy Cal-2 and Pb-Zn ores interspersed by Dol/Cal-3 veinlets; (e) Lumpy Dol-2 and Pb-Zn ores interspersed by Dol/Cal-3 veinlets. Stage 1: Dol/Cal-1, stage 2: Dol/Cal-2, stage 3: Dol/Cal-3.

bright yellow for hydrothermal Cal, bright red for hydrothermal Dol, and dark red for host rocks under Cathode Luminescence, with reticulate carbonate minerals in this stage showing overall bright red indicating high dolomite content (Fig. 6g and i).

The syn-sulfide stage 2 consists of Sp-1, Gn-1, Py-2, Dol-2, Cal-2, and Qtz. Macroscopically, Cal-2 occurs in two forms: as aggregates and crystal clusters (Fig. 5a and i), and is associated with sulfides; Sp-1 is typically veined; Gn-1 occurs as veins and masses; Py-2 occurs as masses. Microscopically, granular Py-2 is enclosed by Sp-1 (Fig. 7f), with some growing along fractures in Sp-1 and others occurring in veined structures (Figs. 7d, f, g, and 8g); Gn-1 is in granular form (Fig. 8e), with some Gn-1 grains altered by hydrothermal Dol/Cal-2 and Py-2 (Figs. 6b, 7a, e, and 8g), while others are altered by Sp-1 and Qtz (Figs. 6f and 8f); Dol/Cal-2 coexists with granular Py-2, Sp-1, and vein-like Gn-1 (Figs. 6a-b, d-e, g, and 8h); quartz alters some Sp-2 (Fig. 8b and e); in Cathode Luminescence, hydrothermal calcite appears as bright yellow aggregates/spots (Fig. 6h).

During the stage 3, the mineral assemblage includes Sp-2, Gn-2, Py-3, Cal-3, and Dol-3. Gn-2 occurs as fine veins (Fig. 8e), with some interspersed with hydrothermal Cal-2 (Fig. 7e), some growing along sulfide fractures (Fig. 8c), and some growing along pyrite fractures in veined structures (Fig. 8d and h); Sp-2 is veined; Py-3 occurs in granular and veined forms, with pyrite grains growing along the edges of veined carbonate minerals (Fig. 6h and i); carbonate minerals are veined, interspersed with mineral aggregates, hydrothermal calcite (Fig. 4e and f), and ore minerals (Figs. 5b, f, 6a-c-e, 7f, h, and 8g). During this stage, the carbonate mineral veins mostly appear bright red, indicating high content of hydrothermal dolomite (Fig. 6g).

4.5. Ore grades

The ore grades of the Maoping deposit are very high. For example, in No. I ore bodies, the Pb grades range from 2.64 wt.% to 13.1 wt.% (average 5.46 wt.%), and Zn grades range from 3.90 wt.% to 30.9 wt.% (average 12.81 wt.%). The average grade of Pb and Zn in No. II ore bodies is 5.75 wt.% and 15.8 wt.% respectively. For No. VI ore bodies (He Y et al., 2023), the Pb grade ranges from 0.11 wt.% to 13.98 wt.% (average 7.01 wt.%), while the Zn grade ranges from 0.24 wt.% to 27.38 wt.% (average 17.21 wt.%). The ore grades of some ore bodies can reach up to 40 wt.%, with an average ore grade of 12–30 wt.% (Zou HJ et al., 2004).

5. Discussion

5.1. Mineralization age

Calcite has $^{238}U/^{206}Pb$ ratios ranging from 0.01 to 25.07

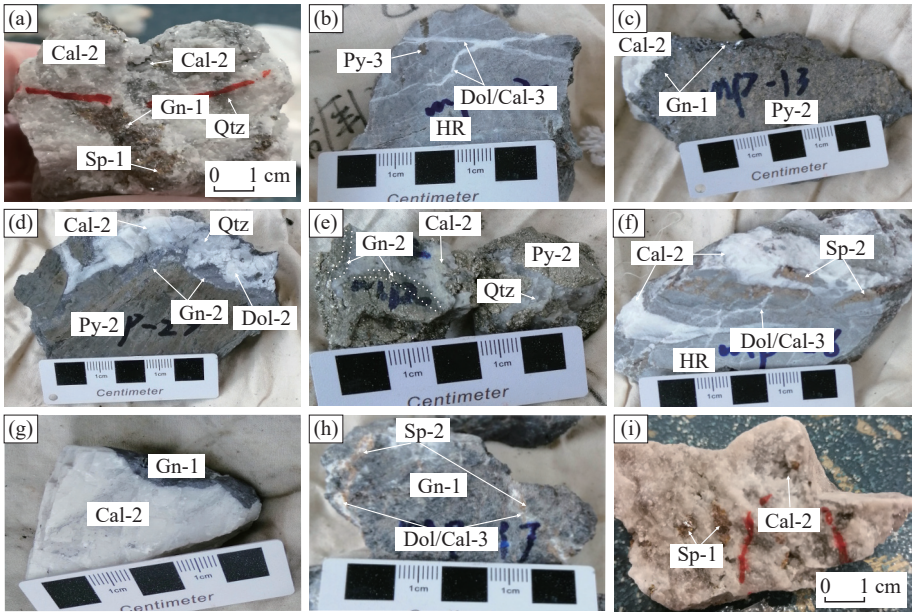

Fig. 5. Photographs of hand specimens from the Maoping deposit. (a) Two forms of calcite: agglomerates and clusters of holes, banded Sp-2 and granular Gn-1; (b) Banded Py-3 interspersed by Dol/Cal-3 veinlets; (c-d) Massive Py-2 and lumpy Dol/Cal-2 intersperses with banded Gn-2; (e) Massive Py-2 coexists with lumpy Cal-2 and Qtz; (f) Banded Sp-1 intersperses with Dol/Cal-1 veins and is interspersed by Dol/Cal-3 veinlets; (g) Massive Gn-1 coexists with lumpy Cal-2; (h) Massive Gn-1 and banded Sp-1 interspersed by Dol/Cal-3 veinlets; (i) Crystal hole clustered calcite, reddish brown Sp-1. stage 1 pyrite (Py-1), stage 2 pyrite (Py-2), stage 2 sphalerite (Sp-1), galena (Gn-1), stage 3 pyrite (Py-3), sphalerite (Sp-2), galena (Gn-2).

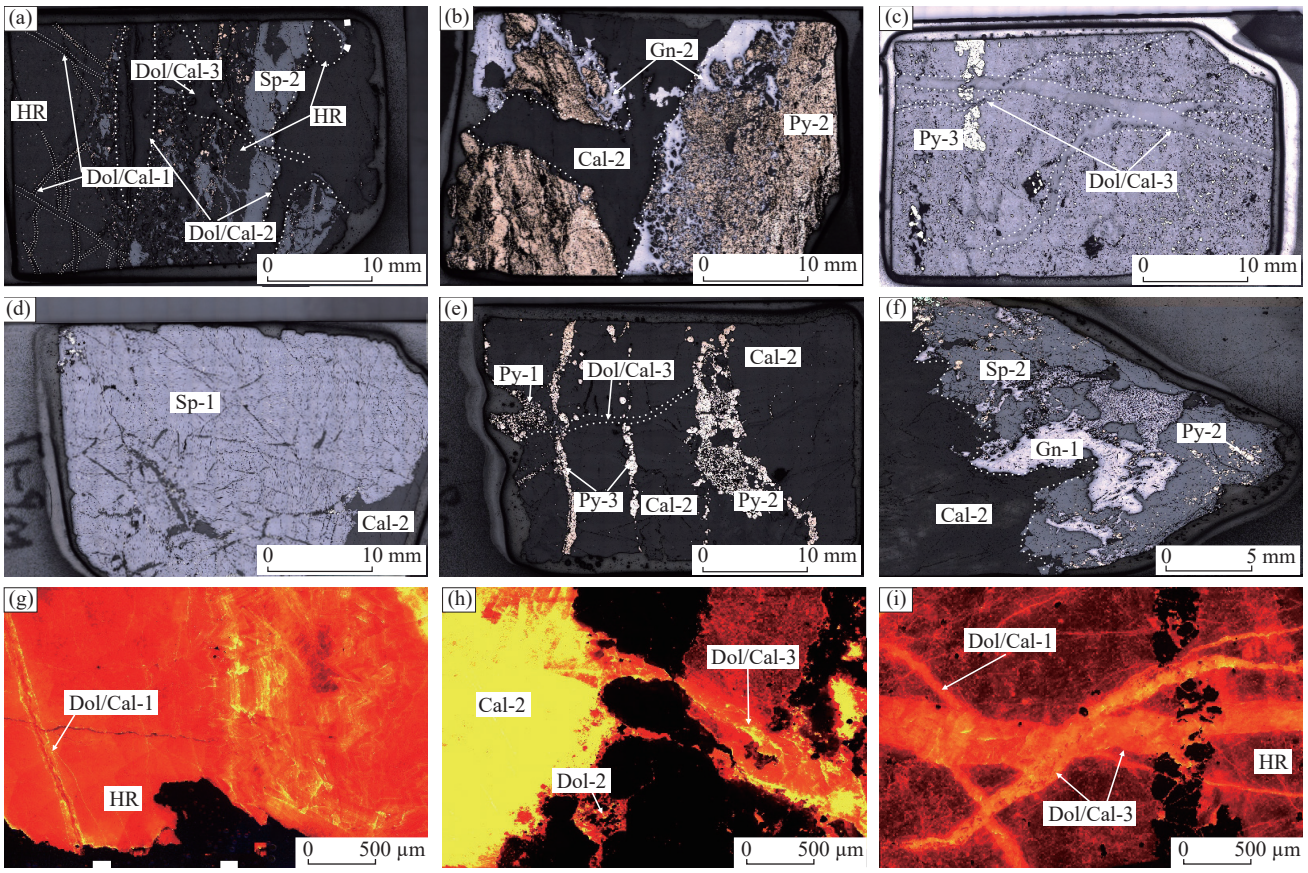

Fig. 6. Textural and structural features of minerals in the Maoping Pb-Zn deposit. (a) Dol/Cal-1 veinlets within HR, and star shaped Py-1, and banded Sp-2 coexists with Dol/Cal-2; (b) Py-2 coexists with Cal-2, Banded Gn-2 interspersed with Py-2; (c) Banded Py-3 interspersed by Dol/Cal-3 veinlets; (d) Cataclastic Sp-1 coexists with Cal-2; (e) Banded Py-2 coexists with Cal-2 and intersperses Dol/Cal-1 veins, but Py-3 is interspersed by Dol/Cal-3 veinlet; (f) Gn-1 is associated with Cal-2, and is partially replaced by Sp-2, and Py-2 is fragmentary (g) Sulfides intersperse with Dol/Cal-1 stockwork with high content dolomite; (h) Cal-2 is bright yellow and coexists with sulfides; Dol-2 is bright red and coexists with sulfides; Dol/Cal-3 vein with high content dolomite intersperse with sulfides; (i) Dol/Cal-1 stockwork with high content dolomite; Dol/Cal-3 vein with high content dolomite intersperse with sulfides.

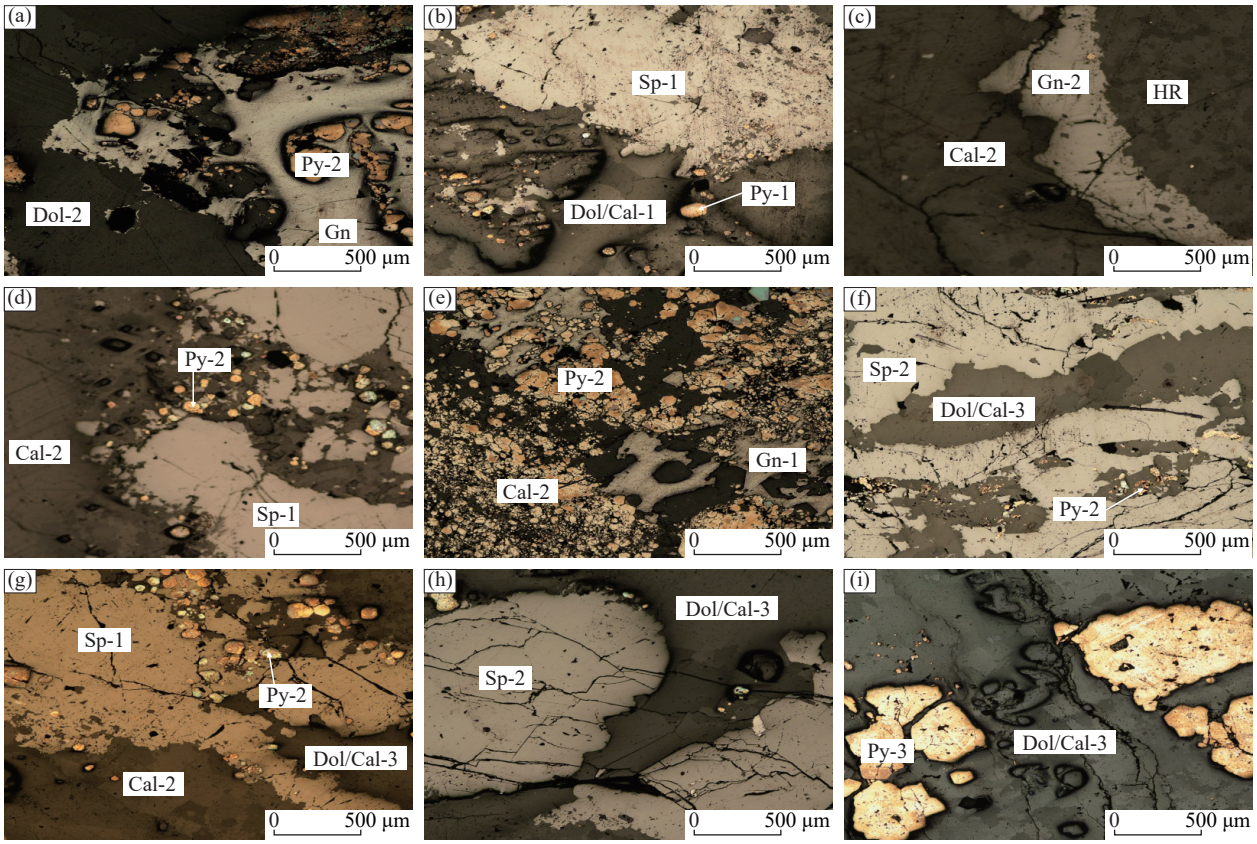

Fig. 7. Textural and structural features of minerals in the Maoping deposit under a microscope. (a) Gn-1 replaces Py-2, and both coexists with Dol-2; (b) Hypidiomorphic-xenomorphic Py-1 coexists Dol/Cal-1 veinlets in the HR, but both interspersed by Sp-1; (c) Cal-2 coexists with banded Gn-2; (d) Cal-2 coexists with Sp-1, and replaces granular Py-2; (e) Cal-2 coexists with Gn-1, and both replace fragmentary Py-2; (f-h) Sp-2 coexists with granular Py-2 and Cal-2, but interspersed by Dol/Cal-3 veinlets; (i) Py-3 replaced by Dol/Cal-3 veinlets.

(Table S2), and shows a sufficiently large variation that allows for the definition of an isochron on the Tera-Wasserburg Concordia diagram.

The metallogenic age is an important basis for understanding the genesis of mineral deposits. Although many methods have been implemented for the dating of the Maoping deposit, several contradicting ages have been obtained. For example, previous sphalerite Rb-Sr dating yielded three distinct isochron age ranges of 448 ± 4 Ma, 322-305 Ma, and 203-202 Ma for the Maoping Pb-Zn deposit (Shen ZW et al., 2016; Yang Q and Zhang J, 2018; Yang B et al., 2018; Yang Q, 2021).

In this study, analytical sample spots plot in the $^{238}U/^{206}Pb$-$^{207}Pb/^{206}Pb$ diagram with a mean standard weighted deviation (MSWD=1.5) in the $^{238}U/^{206}Pb$ vs. $^{207}Pb/^{206}Pb$ diagram (Fig. 9a), indicating an accurate regression due to a good closed system (Luo K et al., 2020a). The U-Pb dating was conducted on hydrothermal calcite as confirmed by the REEs profile and C-O isotope signatures. The calcite that coexists with sphalerite and galena occur either as agglomerates or clusters of crystal holes.

Clustered calcite has a narrow range of U/Pb ratios (U/Pb=0.001-7), whereas clustered calcite has a range of U/Pb ratios (U/Pb=0.04-25). The clustered calcite analyzed formed in a closed hydrothermal system with sulfides and has a low initial Pb content, as evidenced by the accuracy of the age data (Figs. 9, Tables S1 and S2). In this contribution, our new LA-ICPMS U-Pb in-situ analyses yielded an age of 214 ± 20 Ma for hydrothermal calcite, suggesting that the Maoping deposit is possibly formed during the Late Triassic.

In addition, based on fluorite and calcite Sm-Nd, and sphalerite Rb-Sr dating, many other Pb-Zn deposits in the Upper Yangtze province (Table S3) are recognized to be formed during the Late Triassic.

For example, the Jinshachang Pb-Zn deposit with a fluorite Sm-Nd age of 201 ± 3 Ma and a sphalerite Rb-Sr age of 200 ± 5 Ma (Mao JW et al., 2012), the Lehong Pb-Zn deposit with a sphalerite Rb-Sr isochron age of 201 ± 2 Ma (Zhang YX et al., 2014), the Daliangzi Pb-Zn deposit with a calcite Sm-Nd isochron age at 204 ± 1 Ma (Mao JW et al., 2012), and the Huize Pb-Zn deposit with calcite Sm-Nd isochron ages of 225 ± 38 Ma to 226 ± 15 Ma and sulfides Rb-Sr isochron ages of 225 ± 3 Ma to 226 ± 3 Ma (Li WB et al., 2004a). The U-Pb isochron age of calcite acquired in this study is consistent with the mineralization ages of these deposits within the error.

Hence, we believe that the U-Pb ages of calcite may represent the formation time of the Maoping deposit, which is synchronous and tectonically associated with the eruption of the Emeishan mantle plume basalts and Indosinian orogeny.

5.2. Source of ore-forming fluids and materials

5.2.1. Source of ore-forming fluids

Trace elements of carbonates from the Maoping deposit

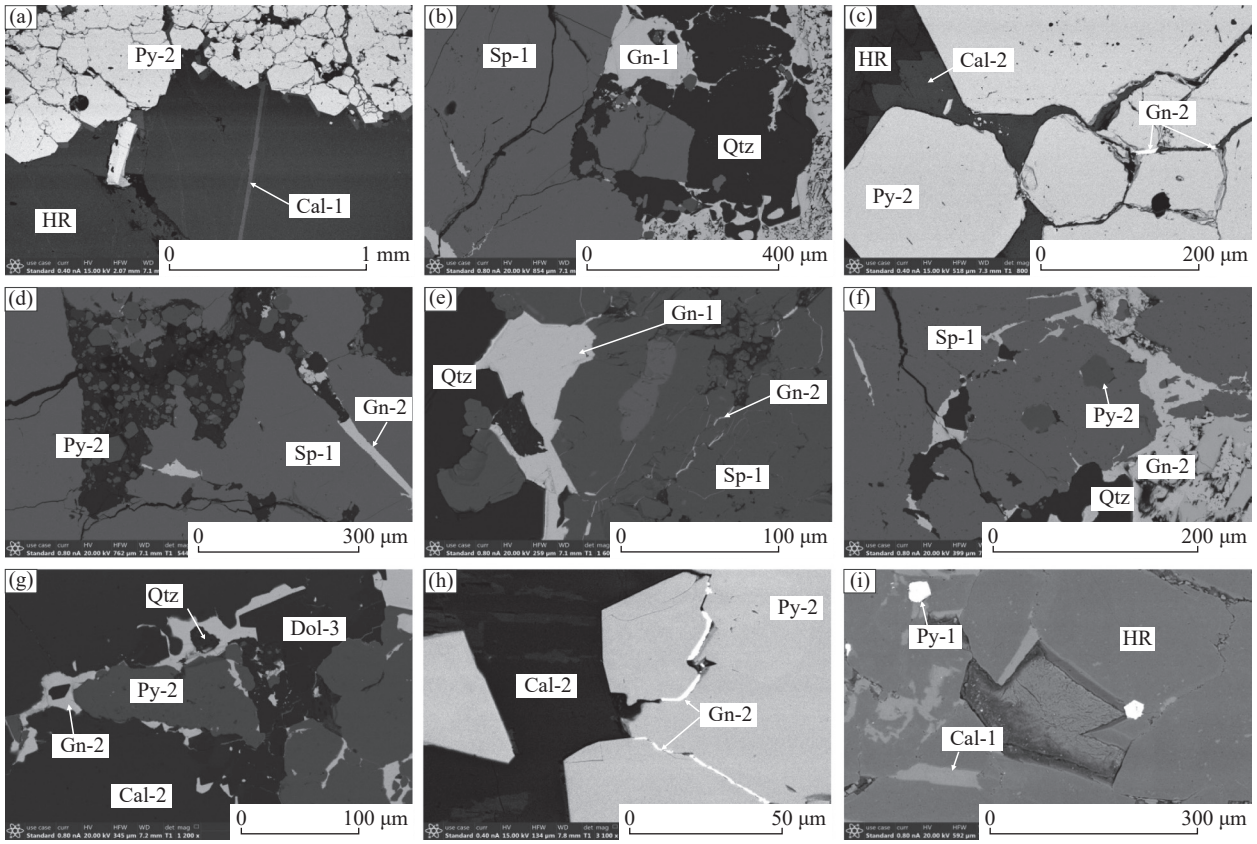

Fig. 8. Textural and structural features of minerals in the Maoping Pb-Zn deposit under a scanning electron microscope (SEM). (a) Cal-1 vein interspersed by Py-2 in host rocks; (b) mineral assemblage: quartz (Qtz) + galena (Gn-1) + sphalerite (Sp-1), Qtz replaces Gn-1 and Sp-1; (c) Cal-2 and banded Gn-2 fill fractures in the Py-2; (d) automorphic-hypidiomorphic granular Py-2 and banded Gn-2 fill fractures in the Sp-1; (e) mineral assemblage: Qtz + Sp-1 + Gn-1; (f) mineral assemblage: Qtz + Gn-2 + Py-2 + Sp-1; granular Py-2 is wrapped by Sp-1; Sp-1 and Qtz replace Gn-2; (g) Cal-2 coexists with Py-2; Dol-3 vein intersperses with Py-2; Py-2 and Cal-2 replace Gn-2 in vein; (h) Cal-2 coexists with Py-2, Gn-2 vein fills fractures in the Py-2; (i) hypidiomorphic Py-1 and vein Cal-1 in host rocks.

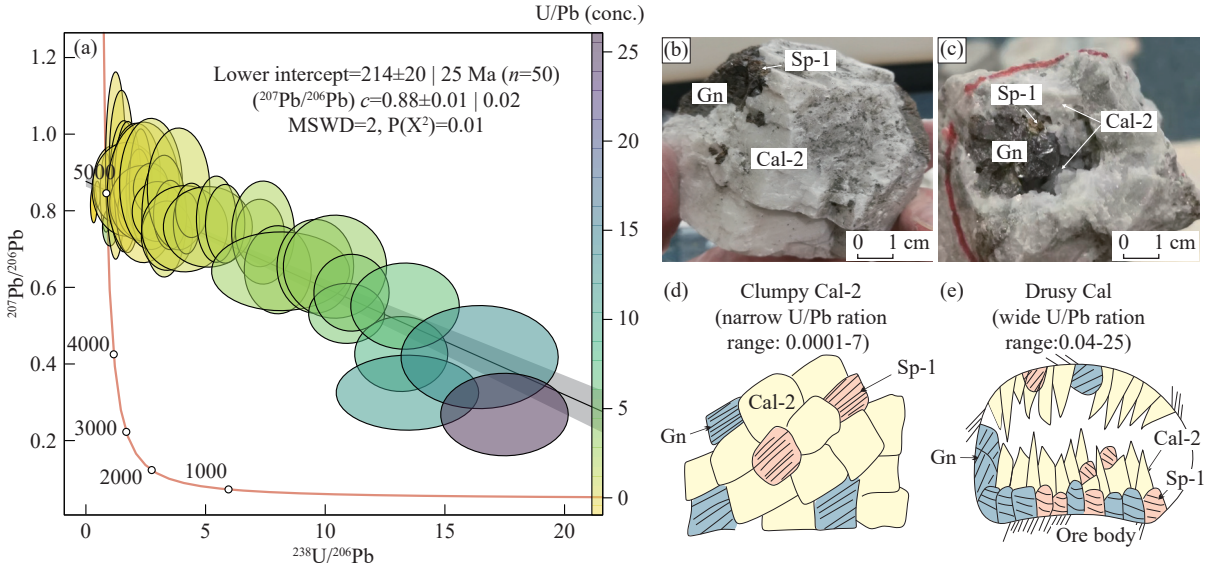

Fig. 9. (a) Tera-Wasserburg concordia diagram ($^{238}U/^{206}Pb$ *vs.* $^{207}Pb/^{206}Pb$) of LA- ICPMS U-Pb ages of Cal-2 from the Maoping deposit. Error ellipses are 2σ, MSWD-mean square of weighted deviates, (b) Massive calcite co-occurring with sphalerite and galena, (c) Crystal-hole clustered calcite co-occurring with sphalerite and galena, and (d-e) Corresponding mineral relationships cartoon.

are shown in Table S4 and illustrated in Figs. 10–11. The carbonates in the host rocks have Fe contents of 415–2207 10^{-6}, Mn contents of 169–724 10^{-6}, and Sr contents of 36.3–72.4 10^{-6}. The total rare earth elements (ΣREE) contents of 8.06–10.7 10^{-6} with ΣLREE/ΣHREE (light rare earth elements/heavy rare earth elements) ratios of 2.61–4.28. The δEu and δCe values are 0.45–1.16 and 0.96–1.34, respectively. The host rocks are characterized by LREE enrichment, with

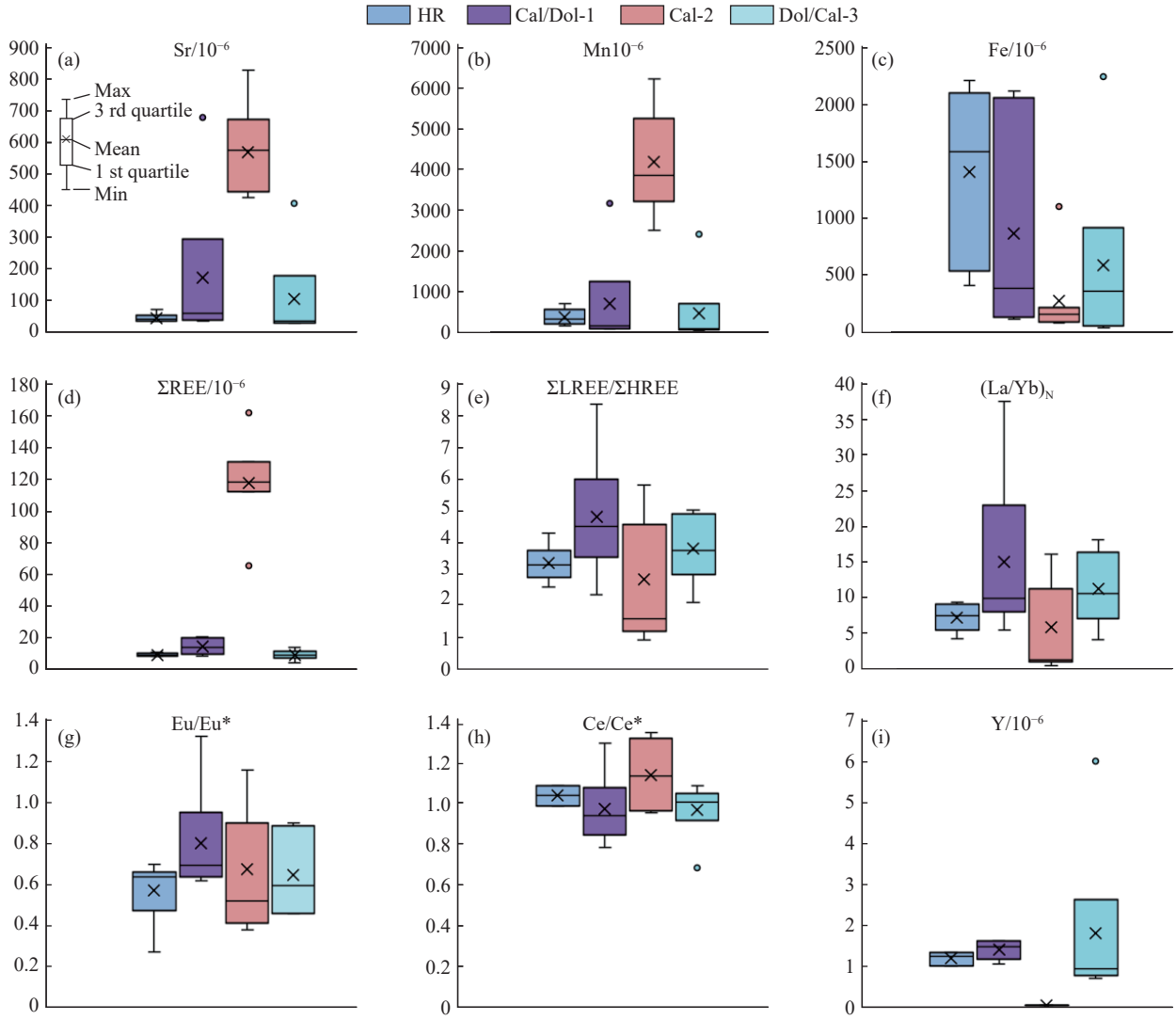

Fig. 10. Box plots of (a) Sr, (b) Mn, (c) Fe, (d) ΣREE, (e) ΣLREE/ΣHREE, (f) $(La/Yb)_N$, (g) Eu/Eu*, (h)Ce/Ce*, and (i) Y values of hydrothermal calcites from the Maoping Pb-Zn deposit.

obvious Eu negative anomalies and insignificant Ce anomalies.

Cal/Dol-1 have Fe contents of 119–2112 10^{-6}, Mn contents of 96.1–3151 10^{-6}, and Sr contents of 37.4–676 10^{-6}. It has ΣREE contents of 8.24–20.4 10^{-6}, and the ΣLREE/ΣHREE ratios of 2.35–8.34. The δEu values of 0.27–0.70, and the δCe values of 0.98–1.31.

The Cal-2 has Fe contents of 86.3–1103 10^{-6}, Mn contents of 2493–6189 10^{-6} and Sr contents of 426–823 10^{-6}. The ΣREE contents of 65.1–161 10^{-6} and the ΣLREE/ΣHREE ratios of 0.93–5.80, with δEu values of 0.46–1.32 and δCe values of 0.86–1.08.

The Cal/Dol-3 has Fe, Mn and Sr contents of 43.7–2240 10^{-6}, 51.8–2418 10^{-6}, and 30.7–406 10^{-6}, respectively. The ΣREE values of 4.05–13.6 10^{-6}, and the ΣLREE/ΣHREE ratios of 2.11–4.86. Their δEu and δCe values are 0.46–0.90 and 0.68–1.29, respectively.

Table 2 presents the results of the C-O isotopes of carbonates from the Maoping deposit. The $\delta^{13}C_{PDB}$ and $\delta^{18}O_{SMOW}$ values of the host rocks range from −1.34‰ to +0.60‰ and +23.69‰ to +26.51‰, respectively. The Cal/Dol-1 samples have $\delta^{13}C_{PDB}$ values ranging from −5.56‰ to +0.26‰ and $\delta^{18}O_{SMOW}$ values of +16.55‰ – +26.77‰ The Cal-2 samples exhibit $\delta^{13}C_{PDB}$ and $\delta^{18}O_{SMOW}$ values ranging from −5.19‰ to −1.03‰ and +13.28‰ – +26.00‰, respectively. In addition, the $\delta^{13}C_{PDB}$ values of the Cal/Dol-3 samples range from −4.07‰ to −1.03‰ and $\delta^{18}O_{SMOW}$ values of +14.28‰ – +24.86‰.

The metalliferous underlying strata are an important mineral source for the mineralizing system.

Carbonates are the primary carriers of REE with their REE contents may be more than two orders of magnitude higher than the one of sulfides (Zhou JX et al., 2012, 2018b; Luo K et al., 2019). Therefore, the REE characteristics of carbonates is used to track the source of REE in the hydrothermal system.

The Cal-2, which is synchronous with the mineralization, is enriched in REE (Fig. 11a), which is significantly higher than the Cal-1 that form at an earlier stage. The REE features indicate that some REE were carried by the mineralizing fluids. The Eu is more sensitive to temperature and fluid reducibility, and with the mineralization progress, the

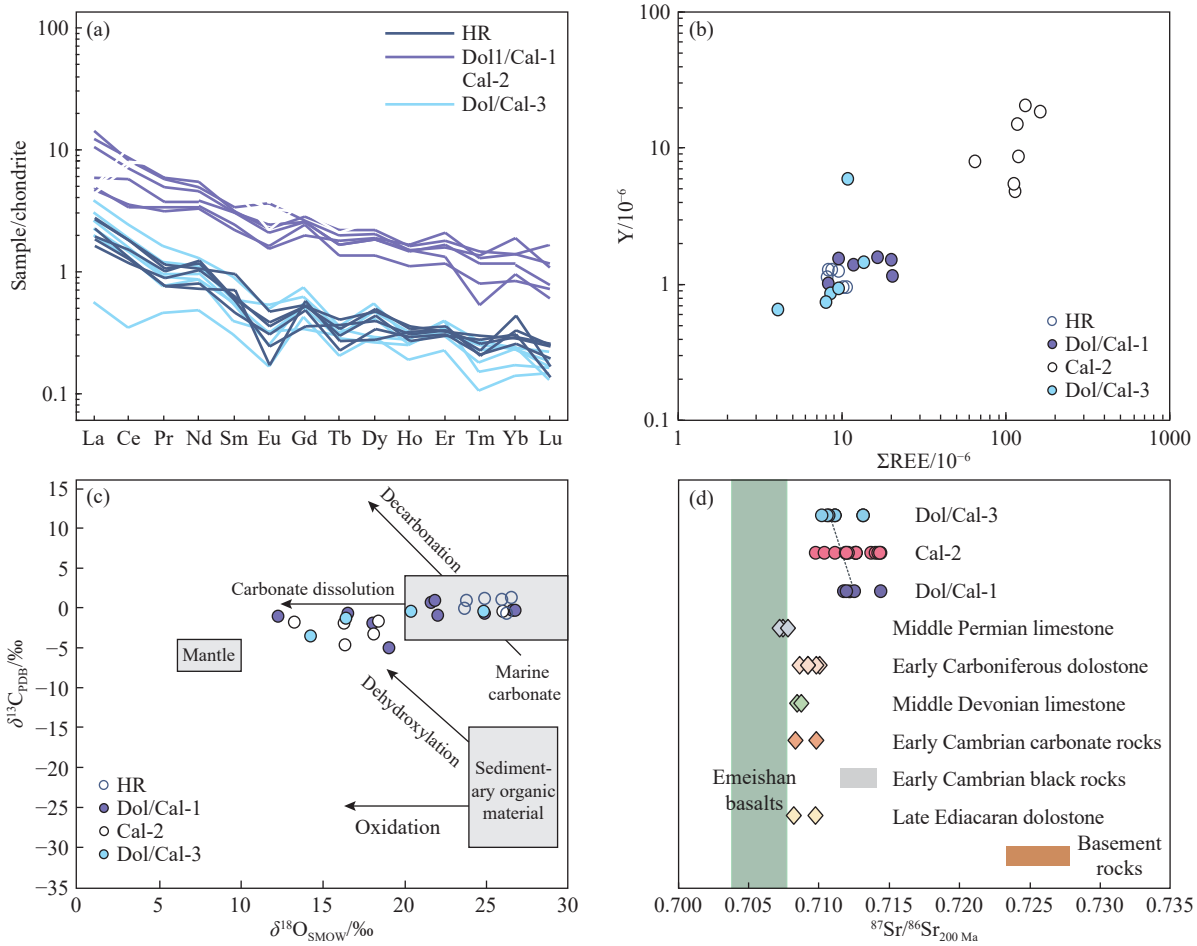

Fig. 11. (a) Distribution model of rare earth elements, (b) Y-ΣREE diagram of carbonate host rocks and hydrothermal carbonate minerals, (c) distribution range of C-O isotopes of carbonate host rocks and hydrothermal carbonate minerals, (d) comparison plot of $^{87}Sr/^{86}Sr_{200Ma}$ ratios between hydrothermal minerals and sedimentary rocks. Data are from Zhou JX et al. (2018a), Deng HL et al. (2000), Shi H et al. (2003), Jiang YH and Li SR (2005), and Chen HS and Ran CY (1992).

temperature gradually decreases. Hence, in comparison to temperature, the presence of intense reducing conditions during the mineralization process could be the pivotal factor leading to notable Eu negative anomalies. The reduction of Eu^{3+} to Eu^{2+} increases the ion radius and restrain Eu to replace Ca^{2+} into the crystal lattice of carbonates, resulting in a negative Eu anomaly for hydrothermal calcite (Bau M and Moeller P, 1992). The Ce is more sensitive to pH value. Under slightly acidic condition, Ce^{3+} in the fluid is easily reduced to insoluble Ce^{4+}, which enters hydrothermal calcite, leading to negative Ce anomaly (Lottermoser BG, 1992). From the stages 1 to 3, Eu is described by a more negative anomaly while Ce in Cal-2 shows a positive anomaly, which reflects the pH decrease.

The Dol/Cal-1 and Dol/Cal-3 show similar REE compositions to those of the ore-hosting rocks. They all plot in the same area in the Y vs. ΣREE diagram (Fig. 11b), indicating that the carbonates of the stages 1 and 3 were derived from the dissolution of the host rocks. However, the Cal-2 has much higher ΣREE + Y contents than those of the host rocks, Dol/Cal-1 and Dol/Cal-3 (Fig. 11b), which suggests the REE of Cal-2 may be added by the underlying strata.

An effective way to identify the source of the ore-forming fluids is to determine C-O isotopes of hydrothermal carbonates (Zheng YF et al., 2001). Previous studies have shown that C-O isotopes in hydrothermal fluids dominantly originated from three sources: (1) mantle degassing or magmatism, with $\delta^{13}C_{PDB}$ values ranging from −8‰ to −4‰ and $\delta^{18}O_{SMOW}$ values ranging from +6‰ to +10‰ (Taylor HP et al., 1967); (2) organic matters in various sedimentary rocks, with $\delta^{13}C_{PDB}$ values of −30‰ to −15‰ and $\delta^{18}O_{SMOW}$ values of +24‰ to +30‰ (Hoefs J, 2004); (3) marine carbonate rocks, with $\delta^{13}C_{PDB}$ values ranging from −4‰ to +4‰ and $\delta^{18}O_{SMOW}$ values ranging from +2‰ to +30‰ (Veizer J and Hoefs J, 1976). The host rocks have $\delta^{13}C_{PDB}$ values ranging from −1.34‰ to +0.60‰ and $\delta^{18}O_{SMOW}$ values ranging from +23.69‰ to +26.51‰, and plots in the region of marine carbonates (Fig. 11c), indicating their marine sedimentary origin. Most of the Cal/Dol-1 falls within the region of marine carbonate rocks, and some left deviate along the curve of carbonate dissolution, indicating that their affinity to the host rocks. However, most of the Cal-2 and Cal/Dol-3 plot in the area between marine carbonate rocks and mantle and left deviate along the carbonate dissolution curve (Fig. 11c). The big variation of $\delta^{18}O_{SMOW}$ values of the Cal-2 and Cal/Dol-3

Table 2. C-O isotopic compositions of carbonate minerals in the Maoping Pb-Zn deposit.

No.	Stage/Object	Stratum	$\delta^{13}C_{PDB}$/‰	$\delta^{18}O_{SMOW}$/‰
MP-1	Carbonate wall rocks	Zaige Formation	−1.34	26.21
MP9-1			0.60	26.51
MP9-2			0.30	23.78
MP10		Weining Formation	−0.65	23.69
MP19-2			0.56	24.90
MP20			0.44	25.94
MP-2	Stage 1 Cal/Dol-1	Zaige Formation	−1.28	24.91
MP-3			−5.56	19.07
MP-5			−0.92	26.58
MP-5			−1.51	22.07
MP-7			−0.92	26.77
MP8-2			−1.29	16.55
MP-16		Weining Formation	0.01	21.60
MP-18			−2.48	18.06
MP21		Weining Formation	0.26	21.86
MP2-6	Stage 2 Cal-2	Zaige Formation	−1.03	26.00
MP11			−5.19	16.40
MP15			−2.35	13.28
MP17		Weining formation	−2.50	16.31
MP23			−2.28	18.44
MP24			−3.85	18.13
MP-14	Stage 3 Cal/Dol-3	Zaige Formation	−4.07	14.28
MP22		Weining Formation	−1.03	24.86
MP22-1			−1.91	16.43
MP22-2			−1.09	20.39

Note: Dol-dolomite; Cal-calcite.

(+13.28‰ to +26.00‰) indicates a complex formation process. Combined with previous studies, it is believed that the distribution trend of the sample falling point is mainly related to related to water/rock reaction and CO_2 degassing (Zheng YF, 1990; Wang LJ et al., 2012; Luo K et al., 2019).

5.2.2. Source of ore-forming elements

Sulfur (S) isotopes: This study collected sulfur isotopes of barite, surrounding rocks, and sulfides from 14 typical ore deposits in the Upper Yangtze province (Table S5; Fig. 12), and 27 typical MVT ore deposits from abroad (Leach DL et al., 2005). The ore deposits in the Upper Yangtze province are found in marine carbonate rocks ranging from the Cambrian to Permian periods.

The $\delta^{34}S$ values of metal sulfides in MVT Pb-Zn deposits are generally close to contemporaneous sulfate $\delta^{34}S$ values, with most $\delta^{34}S$ values being <+20‰, although some deposits exhibit $\delta^{34}S$ values >+20‰ (Fig. 12). The sulfur isotopes of MVT Pb-Zn deposits globally show considerable variation but overall exhibit crustal characteristics (Fig. 12a; Leach DL et al., 2005), whereas those Pb-Zn deposits in the Upper Yangtze province show slight differences, with some deposits lacking crustal characteristics (Fig. 12b). For individual deposits or regions, sulfur may have a single or multiple sources, such as evaporite rocks containing sulfates, coeval seawater, syn-sedimentary sulfates, sulfur-containing organic matter, H_2S gas reservoirs, and reduced sulfur in anoxic basin waters.

The data collected for the Maoping Pb-Zn deposit mainly fall within the ranges of −24‰ to −8‰ and +8‰ to +28‰, with the majority falling within the +8‰ to +24‰ range, and an average value of +16.6‰ (Fig. 13a). The $\delta^{34}S$ values of sulfides in other deposits in the region mostly range from +9.0‰ to +18.0‰, significantly higher than mantle-derived magmatic sulfur (about 0‰: Chaussidon M et al., 1989), indicating that the basalts in the region are unlikely to have provided a significant sulfur source for mineralization. The evaporite gypsum layers rich in gypsum and heavy spar in the adjacent Pb-Zn deposits cluster in the Upper Yangtze province have $\delta^{34}S$ values ranging from +12.9‰ to +28‰ (Huang ZL et al., 2004; Zhou JX et al., 2013c), while the $\delta^{34}S$ values of contemporaneous seawater sulfates in the Cambrian to Permian period range from +11‰ to +32‰ (Seal RR, 2006). The $\delta^{34}S$ values of sulfides in the Maoping deposit and other typical deposits in the region are very close to the $\delta^{34}S$ values of evaporites in the Cambrian to Permian strata, suggesting that evaporites in the sedimentary rocks from the Cambrian to Permian periods may have been the primary sulfur source for mineralizing fluids. On a global scale, the majority of MVT deposits also derive their reduced sulfur primarily from the reduction of marine sulfate (Leach DL et al., 2010). In conclusion, the sulfur in the Maoping deposit mainly originates from the reduced sulfur in evaporites in the surrounding rocks.

In the Upper Yangtze province, most Pb-Zn deposits have $\delta^{34}S$ values of sulfides lower than those of the sulfates, but they are very close to those resulting from Thermochemical Sulfate Reduction (TSR) and Bacterial Sulfate Reduction (BSR). For example, the $\delta^{34}S$ values of the sulfides from the Maoping deposit are significantly enriched in heavy sulfur isotopes, closely matching the range of values resulting from BSR, but most of them falling entirely within the range of values resulting from TSR (Fig. 13b). Therefore, in the study area, the main mechanism for the formation of reduced sulfur in most Pb-Zn deposits is TSR, while BSR may be the reason for the lower $\delta^{34}S$ values observed.

Lead (Pb) isotopes: in this study, 269 valid Pb isotopes from the Maoping Pb-Zn deposit were collected. The ranges of $^{206}Pb/^{204}Pb$ = 18.247 to 18.914 (mean 18.695), $^{207}Pb/^{204}Pb$ = 15.400 to 15.802 (mean 15.759), and $^{208}Pb/^{204}Pb$ = 38.548 to 39.530 (mean 39.324) were obtained (Table S6). The small variations in the data range indicate that the Pb isotopes in the Maoping Pb-Zn deposit have a single ore-forming material source or have undergone homogenization (Huang ZL et al., 2004). The ore-hosted strata of the Maoping deposit belong to the Devonian-Carboniferous series. After the Pb isotopes 200 Ma age-corrected, the Permian Emeishan basalts, the Devonian-Carboniferous sedimentary rocks, and the Precambrian metamorphic basement rocks, as well as the sulfide ore minerals, were compared and analyzed in a Pb isotope construction model diagram (Zartman RE and Doe BR, 1981). It was found that almost all the Pb isotope data of

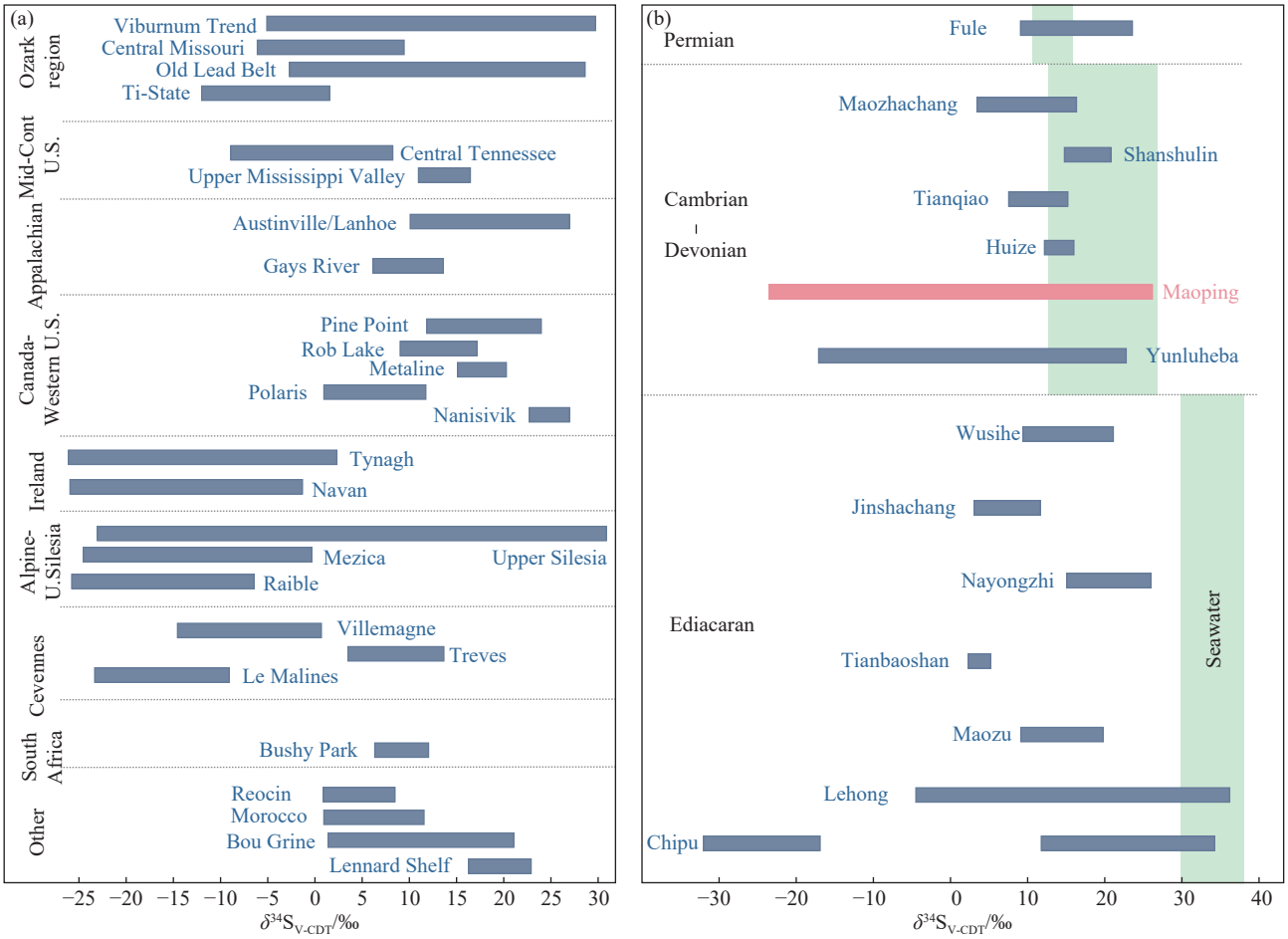

Fig. 12. Distribution map of S isotopes of foreign MVT Pb-Zn deposits; (b) Distribution map of S isotopes of MVT Pb-Zn deposits in the Upper Yangtze province. Data for foreign deposits are from Leach DL et al. (2005). Data for domestic deposits are from He YF et al. (2020); Ren SL et al. (2018); Xiang ZZ et al. (2020); Tan SC et al. (2019a, 2019b); Wang L et al. (2023); Xu SH et al. (2023); Yang Q et al. (2019); Yang Q (2021); Zhao WC et al. (2023); Guo X (2012); Liu HC and Lin WD (1999); Wang T (2018); Shen TLY et al. (2011); Miao Y et al. (2023); Zhou JX et al. (2011, 2013a, 2013b, 2013d, 2014a, 2014b, 2018a); Jin ZG et al. (2016); Zhang YX et al. (2014); Bai JH et al. (2013); Luo K et al. (2022); Zhang H et al. (2016); Zhu CW et al. (2018).

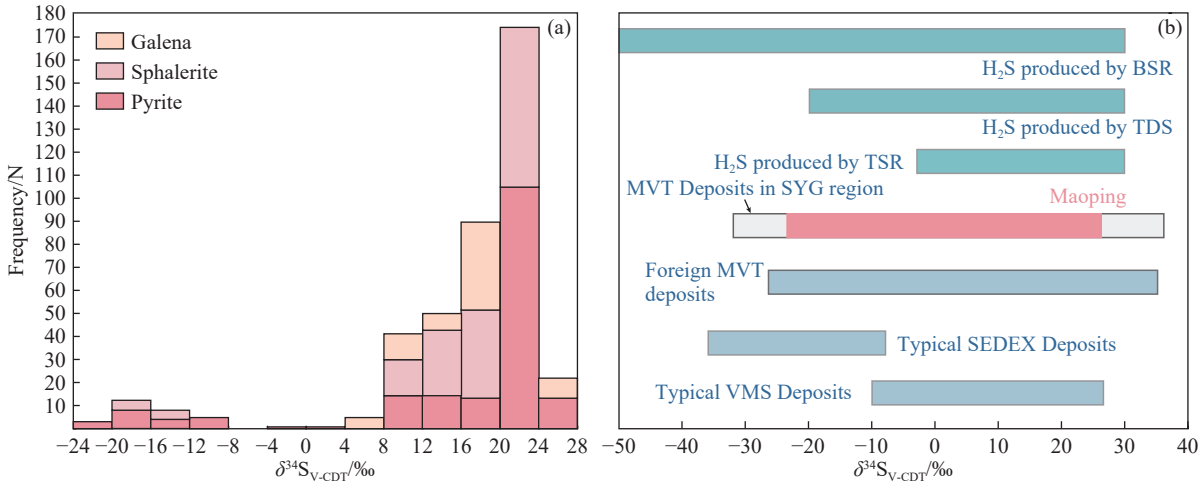

Fig. 13. (a) Histogram of S isotopes distribution of the Maoping deposit; (b) Comparison of $\delta^{34}S$ values of different types of Pb-Zn deposits and related geological bodies; $\delta^{34}S$ values of TSR, BSR, and TDS are from Chen X and Xue CJ (2016).

the ore minerals from the Maoping Pb-Zn deposit fall within the range of Pb isotopes of the sedimentary rocks of the ore-hosted strata and the basement rocks above the average crustal Pb evolution line, forming a sharp angle area within the range of Pb isotopes of the basement rocks and the Devonian-Permian sedimentary rocks, with some falling within the basement rocks and a few in the basaltic rocks area (Fig. 14a). They also fall between the modern Pb isotopes of the upper

crust and lower crust end-members (Fig. 14a and b), indicating a crustal source characteristic of the mineralization metals, showing that the major source of the mineralization metals in the Maoping Pb-Zn deposit is the Devonian-Carboniferous sedimentary rocks, followed by the Precambrian basement rocks, with a small amount possibly souring from the Permian Emeishan basalts.

Strontium (Sr) isotopes: $^{87}Sr/^{86}Sr_{200Ma}$ ratios of carbonates from the Maoping deposit are listed in Table 3. The Cal/Dol-1 has $^{87}Sr/^{86}Sr_{200Ma}$ ratios varying from 0.7119 to 0.7143 with a mean of 0.7126. The Cal-2 has a range of 0.7100 to 0.7144 $^{87}Sr/^{86}Sr_{200Ma}$ ratios with a mean of 0.7121. Moreover, the $^{87}Sr/^{86}Sr_{200Ma}$ ratios of the Cal/Dol-3 range from 0.7120 to 0.7137 (mean of 0.7125).

Strontium (Sr) isotopes have been used to trace the origin, migration, and evolution of hydrothermal fluids (Beaudoin G and Chiaradia M, 2016). In the Maoping Pb-Zn deposit, dolomite from the Upper Ediacaran Dengying Formation has $^{87}Sr/^{86}Sr_{200Ma}$ ratios ranging from 0.7083 to 0.7096, and dolomite from the Middle Devonian Qujing Formation has an $^{87}Sr/^{86}Sr_{200Ma}$ ratio of 0.7101. The $^{87}Sr/^{86}Sr_{200Ma}$ ratios of dolomite from the Upper Carboniferous Formation and limestone from the Upper Devonian vary from 0.7087 to 0.7101 and from 0.7083 to 0.7088, respectively (Deng HL et

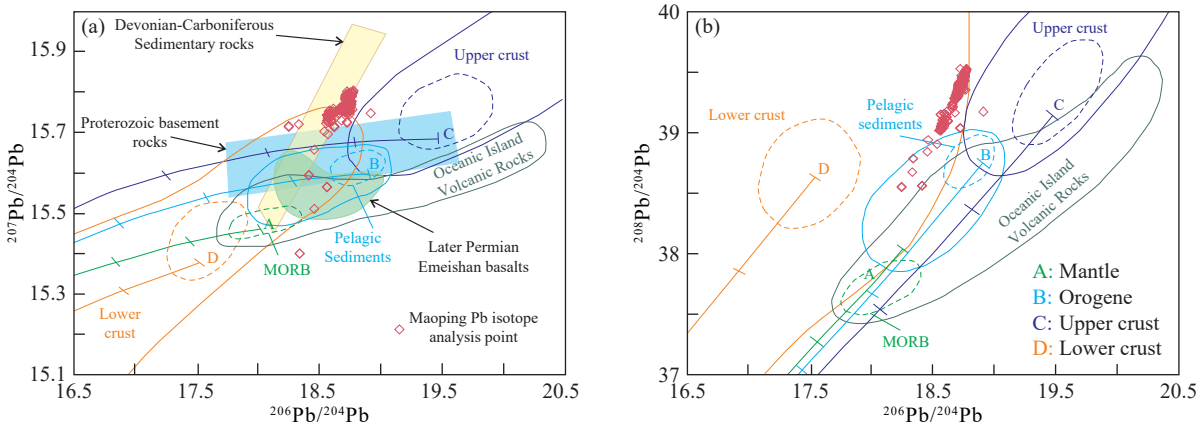

Fig. 14. (a) Comparison of $^{207}Pb/^{204}Pb$ and $^{206}Pb/^{204}Pb$ in Maoping deposit; (b) Comparison of $^{208}Pb/^{204}Pb$ and $^{206}Pb/^{204}Pb$; Pb evolution curves for Mantle (A), Orogenic Belt (B), Upper Crust (C), and Lower Crust (D). Solid lines represent 80% of all data points in each region, and dashed lines represent the mean values (adapted from Zartman RE and Doe BR, 1981). Data for Emeishan basalts, sedimentary rocks, and basement rocks are from Liu HC and Lin WD (1999), Huang ZL et al. (2004) and Zhou JX et al. (2013c).

Table 3. Sr isotopic ratios of carbonate minerals in the Maoping Pb-Zn deposit.

Sample	Stage/Object	$^{84}Sr/^{86}Sr$	2σ	$^{84}Sr/^{88}Sr$	2σ	$^{87}Rb/^{86}Sr$	2σ	$^{87}Sr/^{86}Sr$	2σ
MP-11-2	Stage 1 Cal/Dol-1	0.0580	0.00038	0.0069	0.00004	0.0005	0.00007	0.7143	0.00013
MP5-2-2		0.0581	0.00042	0.0069	0.00005	0.0002	0.00003	0.7122	0.00011
MP5-2-3		0.0586	0.00049	0.0070	0.00006	0.0000	0.00003	0.7126	0.00013
MP5-2-4		0.0572	0.00052	0.0068	0.00006	0.0001	0.00003	0.7120	0.00013
MP5-2-6		0.0580	0.00046	0.0069	0.00005	0.0000	0.00003	0.7119	0.00011
MP11-2-1	Stage 2 Cal-2	0.0575	0.00027	0.0069	0.00003	0.0001	0.00002	0.7143	0.00009
MP11-2-2		0.0576	0.00047	0.0069	0.00006	0.0001	0.00003	0.7140	0.00012
MP11-2-3		0.0581	0.00060	0.0069	0.00007	0.0000	0.00003	0.7142	0.00015
MP11-2-4		0.0584	0.00061	0.0070	0.00007	0.0002	0.00006	0.7144	0.00018
MP-17-1		0.0584	0.00027	0.0070	0.00003	0.0002	0.00003	0.7100	0.00010
MP-17-2		0.0587	0.00034	0.0070	0.00004	0.0002	0.00002	0.7106	0.00011
MP-17-3		0.0586	0.00033	0.0070	0.00004	0.0001	0.00002	0.7113	0.00010
MP-22-1		0.0583	0.00020	0.0070	0.00002	0.0002	0.00003	0.7109	0.00008
MP-22-2		0.0583	0.00020	0.0070	0.00002	0.0001	0.00001	0.7108	0.00007
MP-22-3		0.0582	0.00021	0.0070	0.00003	0.0000	0.00001	0.7104	0.00007
MP-22-4		0.0582	0.00019	0.0070	0.00002	0.0001	0.00001	0.7113	0.00007
MP-22-5		0.0581	0.00022	0.0069	0.00003	0.0002	0.00001	0.7132	0.00007
MP-23-1	Stage 3 Cal/Dol-3	0.0585	0.00028	0.0070	0.00003	0.0002	0.00005	0.7126	0.00011
MP-23-2		0.0578	0.00018	0.0069	0.00002	0.0001	0.00002	0.7120	0.00007
MP-23-3		0.0582	0.00022	0.0069	0.00003	0.0000	0.00001	0.7122	0.00008
MP-23-4		0.0584	0.00027	0.0070	0.00003	0.0004	0.00002	0.7137	0.00010
MP-23-5		0.0575	0.00021	0.0069	0.00002	0.0002	0.00003	0.7120	0.00008
MP-23-6		0.0576	0.00014	0.0069	0.00002	0.0001	0.00001	0.7127	0.00006

Note: Dol-dolomite; Cal-calcite.

al., 2000; Shi H et al., 2003; Jiang YH and Li SR, 2005; Zhou JX et al., 2018a). In addition, the $^{87}Sr/^{86}Sr_{200Ma}$ ratios of limestone from the Middle Permian Qixia-Maokou Formation vary from 0.7073 to 0.7089, those of sand shale of the Lower Permian Liangshan Formation are 0.7167 (Zhou JX et al., 2018a). These Paleozoic carbonate rocks have similar Sr isotopes ($^{87}Sr/^{86}Sr_{200Ma}$ ratios varying from 0.7073 to 0.7167; Fig. 11d). Previous studies have also reported that the metamorphic basements have $^{87}Sr/^{86}Sr_{200Ma}$ ratios varying from 0.7243 to 0.7288 (Chen HS and Ran CY, 1992).

All type of calcite and dolomite has very similar $^{87}Sr/^{86}Sr_{200Ma}$ ratios (Cal/Dol-1 is 0.7119–0.7143, Cal-2 is 0.7100–0.7144 and, Cal/Dol-3 is 0.7120–0.7137). $^{87}Sr/^{86}Sr_{200Ma}$ ratios of Lower Cambrian black rocks (0.7120-0.7136) appear to be higher than those of Upper Mantle (0.704 ± 0.002; Faure G, 1977) and the Emeishan basalts (0.7039–0.7078; Huang ZL et al., 2004; Fig. 13), however, they are lower than those of the metamorphic basements (Chen HS and Ran CY, 1992). These results suggest that the ore-forming fluids have once flowed through a stratigraphy enriched in radioactive Sr (basements), and Upper Cambrian black rocks provided many metallic materials via the water-rock reactions. At the same time, there is a decreasing trend in values from the early to late stages, indicating that the contribution of the basements during the early stage is relatively large, while the contribution of the host rocks during the late stage is relatively large. What's more, water/rock interaction and Sr isotope exchange with shales and clastic rocks ruled out the possibility that mantle and Emeishan basalts could be the main source of metals. Therefore, mantle plume activity may be the thermal force behind the formation of high-grade and large-scale ore bodies.

5.2.3. Formation of carbonate minerals

Carbonates from the Maoping deposit have distinct REE signatures (Fig. 11a and b). Manganese and Sr contents of hydrothermal carbonates are higher than those of the host rocks (Fig. 10). In addition, from the stages 1 to 3, the overall Fe contents of carbonates decrease, indicating that the degree of metasomatism is decreasing. With the decrease of oxygen fugacity and temperatures, the ore-forming environment gradually changes from alkaline to weak acidic.

The solubility of carbonate minerals in the hydrothermal fluids is negatively correlated with temperature and positively correlated with pressure (Holland HD, 1979). Therefore, carbonate minerals precipitation cannot be interpreted solely through cooling in a closed system. In contrast, CO_2 degassing and water/rock interaction are effective means for carbonate minerals precipitation (Du LJ et al., 2017). To estimate the carbon and oxygen isotopic compositions of carbonate minerals in the Maoping deposit, the equilibrium calculation equations for carbon and oxygen isotopic fractionation between calcite and carbon dioxide or water were used (O'Neil JR et al., 1969). The peak homogenization temperature of fluid inclusions was estimated to be 200 °C, and the $\delta^{13}C_{PDB}$ and $\delta^{18}O_{SMOW}$ were concentrated ranging from −5.61‰ to +0.22‰ (average −2.1‰) and from −14.70‰ to +17.76‰ (average +8.9‰).

CO_2 degassing: The batch model proposed by Zheng YF (1990) and Rayleigh model are used to simulate the distribution of carbon and oxygen isotopes in the Maoping deposit, if H_2CO_3 and HCO_3^- are the main carbon species (Fig. 15a and b). The results suggest that dissolved carbon species are dominated by HCO_3^-, with precipitation temperature between 100°C and 250°C. These results are consistent with the past reports (Huang ZL et al., 2004).

Water/rock interaction: As previously proposed in the literature, the water-rock interaction influences the measured C-O isotope signatures of calcite (Zheng YF and Chen JF, 2000). The following formulas are employed for the calculation of C and O isotopes in calcite precipitated from the hydrothermal fluids:

$$\delta^{13}C_{Cal/Dol} = \delta^{13}C^{i}_{fluid} + (R'/w') \cdot \Delta^{13}C_{rock} + 10^{3}\ln\alpha_{Cal/Dol-fluid} \quad (1)$$

$$\delta^{18}O_{Cal/Dol} = \delta^{18}O^{i}_{fluid} + (R/w) \cdot \Delta^{18}O_{rock} + 10^{3}\ln\alpha_{Cal/Dol-fluid} \quad (2)$$

The carbon and oxygen isotopic compositions of the fluids prior to the water/rock interaction are represented by the $\delta^{13}C^{i}_{fluid}$ and $\delta^{18}O^{i}_{fluid}$ values, respectively. The mass ratios of carbon and oxygen atoms between rocks and fluids are indicated as R′/W′ and R/W, respectively. These parameters can be used to calculate the difference between the initial and final isotopic compositions of rocks, which are expressed as $\Delta rock = \delta^{i}_{rock} - \delta^{f}_{rock}$, following the calculation formula for the carbon and oxygen isotopes of calcite precipitated from the hydrothermal fluids.

The results suggest that by using H_2CO_3 and HCO_3^- as the dominant carbon species in the simulation (Fig. 15c), the precipitation of hydrothermal calcite associated with Pb-Zn mineralization is independent of water-rock interaction.

5.2.4. Ore genesis and a metallogenic model

Although numerous studies have explored the characteristics of Pb-Zn deposits in the Upper Yangtze province, the ore genesis of these deposits remains controversial. For example, they are sedimentary-reworked, the Huize-type (Han RS et al., 2007), MVT (Wei AY et al., 2015; He YF et al., 2020; Wu T et al., 2021; Zhao WC et al., 2023) or the MVT-like epigenetic Upper Yangtze-type deposits (Zhou JX et al., 2013a, 2018a).

Undoubtedly, there are many similarities in the ore-forming characteristics between these deposits and the MVT deposits, but the occurrences of Pb-Zn deposits in the province are within compressive zones (reverse fault-anticline technical systems) of passive margin technical settings (western Yangtze Block), and have spatial and genetic (thermal flow, volatile and fluid) associations with the ELIP. Furthermore, these deposits are characterized by high ore grades (>10 wt.% Pb + Zn), high concentrations of associated elements (Cu, Ag, Ge, Ga and Cd), and medium-low temperatures (<300 °C) and salinities (<20 wt.% NaCl equiv.). Hence, this study believes that it belongs to the MVT-

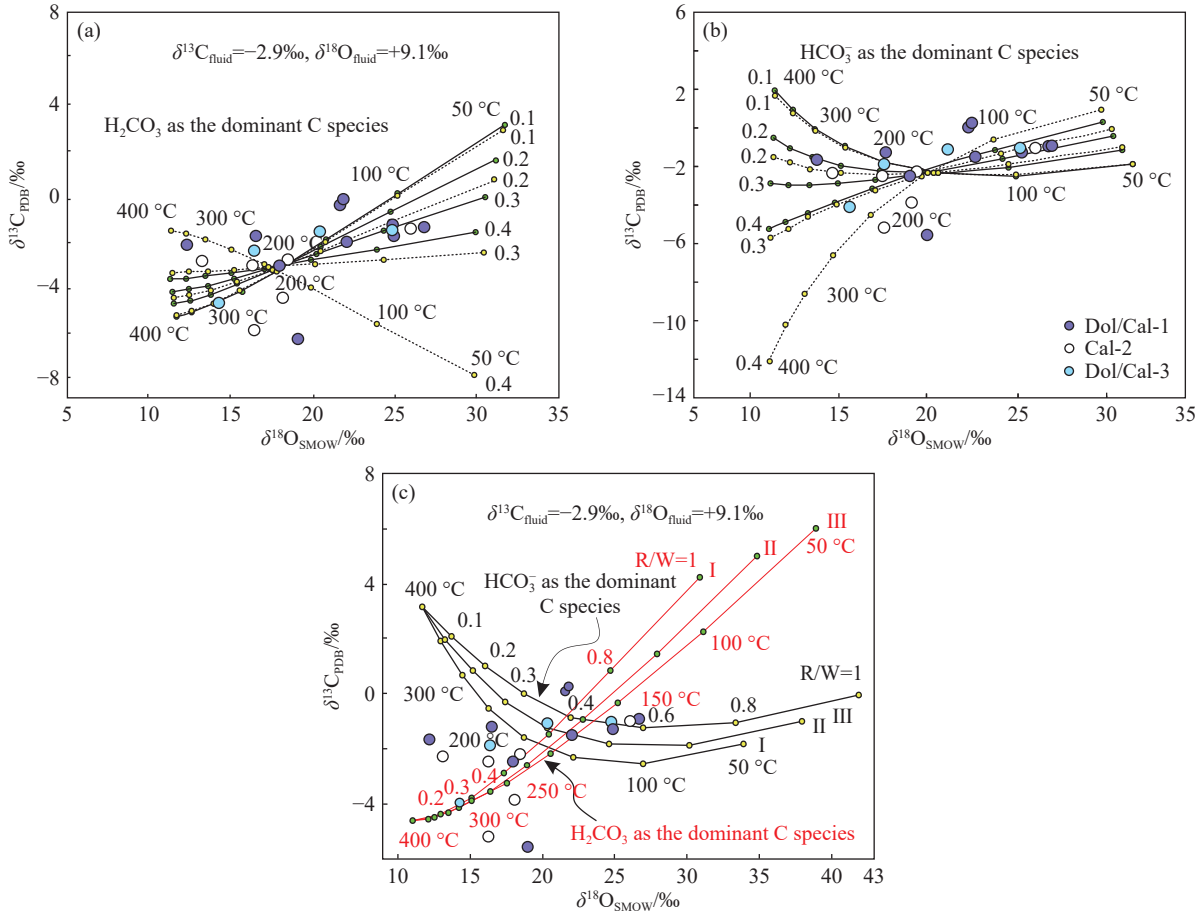

Fig. 15. (a) H_2CO_3 and (b) HCO^{3-} as the dominant carbon species in simulation diagram of CO_2 degassing for the hydrothermal carbonate minerals; (c) simulation diagram of water-rock interaction for hydrothermal carbonate minerals.

like Upper Yangtze-type, which has more guiding significance for mineral exploration (Zhou JX et al., 2018a).

Although different dating methods have been applied to the study of metallogenic chronology of Pb-Zn deposits in the Upper Yangtze province, there is large discrepancy among the ages obtained, ranging from the Paleozoic to the Cenozoic (Table S3 and Fig. 16). However, the age internal that fit better to the regional geotectonic setting is the Mesozoic (Fig. 16), since the mineralization is more likely synchronous to the Indonician tectonic event in South China. During the closure of the Paleo-Tethys Ocean, the collision and compression between the Indochina and South China Blocks created favorable condition for the generation of many low-temperature (120°C-250°C) hydrothermal mineralization within the Western Yangtze Block, SW China (Hu RZ et al., 2017).

A metallogenic model is proposed for the Maoping Pb-Zn deposit (Fig. 17). About 260 Ma, Emeishan mantle plume basaltic magamatism (Zhou MF et al., 2002) provide thermal sources for deep-seated fluids to extract metals from Precambrian basement rocks. This process led to the formation of an initial basin brine fluids. During the closure of the Paleo-Tethys Ocean in the Late Triassic (230-200 Ma) the interaction among the Indochina, South China and North China Blocks formed the Indonisian orogeny, and resulted in the establishment of a compressional tectonic setting beneath SW China (Hu RZ et al., 2017; Zhou JX et al., 2018b; Luo K et al., 2020b). The compressional setting led to the formation of several northwest-oriented thrust faults and folds in the Upper Yangtze province providing convenient channels for the circulation of deep-seated fluids and formation of Pb-Zn mineralization (Hu RZ et al., 2017). In addition, the ore-forming fluids underwent a series of physical and chemical processes such as carbonate dissolution and CO_2 degassing as discussed earlier on, and finally formed large-scale ore bodies with high grades of Pb and Zn hosted by carbonated along secondary faults.

6. Conclusions

(i) The Maoping Pb-Zn deposit has identified 9 groups of ore bodies, with the total quantity of Pb-Zn ores exceeding 41 Mt, with average ore grades of 12-30 wt.% (Pb + Zn metal reserves exceed 5 Mt). It ranks as the second largest Pb-Zn deposit within the Upper Yangtze province and holds the distinction of being the largest Pb-Zn deposit hosted in carbonate rocks of the Devonian-Carboniferous.

(ii) Carbonate minerals (mainly Dol and Cal) are the predominant gangue minerals in the Maoping deposit, forming throughout the entire mineralization process and can be divided into the pre-, syn- and post-sulfide three stages.

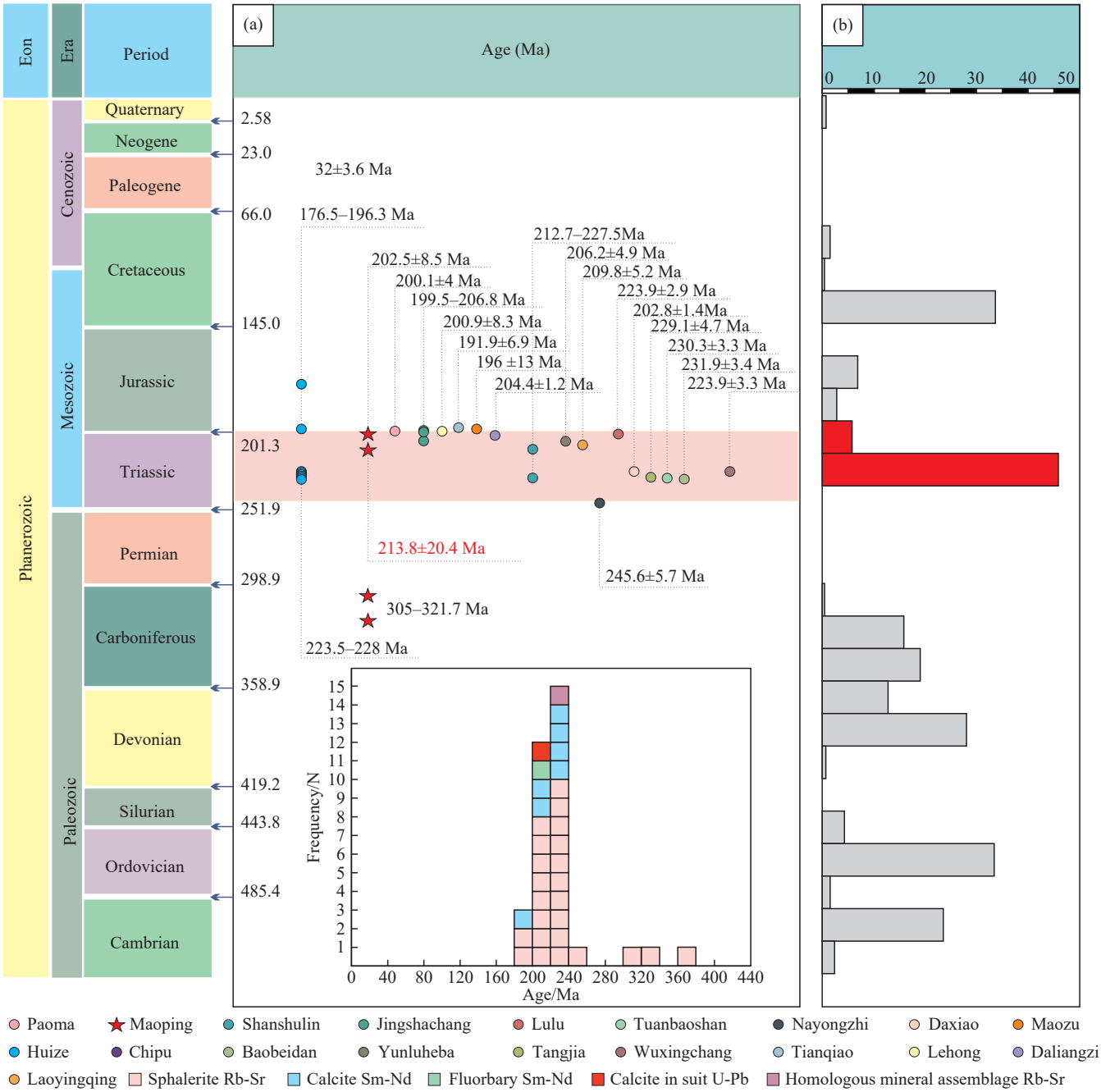

Fig. 16. (a) Statistics on the results of different dating methods for the Pb-Zn deposits in the Upper Yangtze province. Ages are from Huang ZL et al. (2004), Li WB et al (2004a, 2004b, 2007), Yin DM et al. (2009), Liu F (2005), Liu XK et al. (2022), Lin ZY et al. (2010), Mao JW et al. (2012), Wu Y (2013), Zhang CQ et al. (2008, 2014, 2015), Zhou JX et al. (2013a, 2013b, 2015), Shen ZW et al. (2016), Yang Q and Zhang J (2018), Yang B et al. (2018), Yang Q (2021), Wang WY et al. (2017), Tang YY et al. (2019), Liao KL et al. (2020), Guan HM et al. (2020), Gong HS et al. (2021), and this study. (b) Distribution of total contained Zn + Pb metal in global MVT deposits versus the measured mineralization age data during the Phanerozoic (data from Leach DL et al., 2010; modified from Xiong SF et al., 2022).

(iii) During the syn-sulfide stage, carbonate minerals reflect that the enrichment of manganese and strontium in ore-forming fluids, which are likely basin thermal brines. Carbonate minerals in the syn-sulfide stage indicate that the input of ore-forming layer material. As the mineralization process progresses, changes of δEu and δCe suggest that a gradual decrease in mineralization temperature and reduction in the reductive nature of the ore-forming environment. The content of Fe indicates a decrease in metasomatism degree. With decreasing oxygen fugacity and temperature, the ore-forming environment gradually transitions from weakly alkaline to weakly acidic.

(iv) The C-O isotopes of the surrounding carbonate rocks fall within the range of marine carbonate rocks, while the C-O isotopes of hydrothermal carbonate minerals away from the distribution range of marine carbonate rocks, indicating that the formation of carbonate minerals through dissolution of marine carbonate rocks. The precipitation mechanism of carbonate minerals in the main ore-forming stage is mainly controlled by the degassing of CO_2 with HCO_3^- as the main

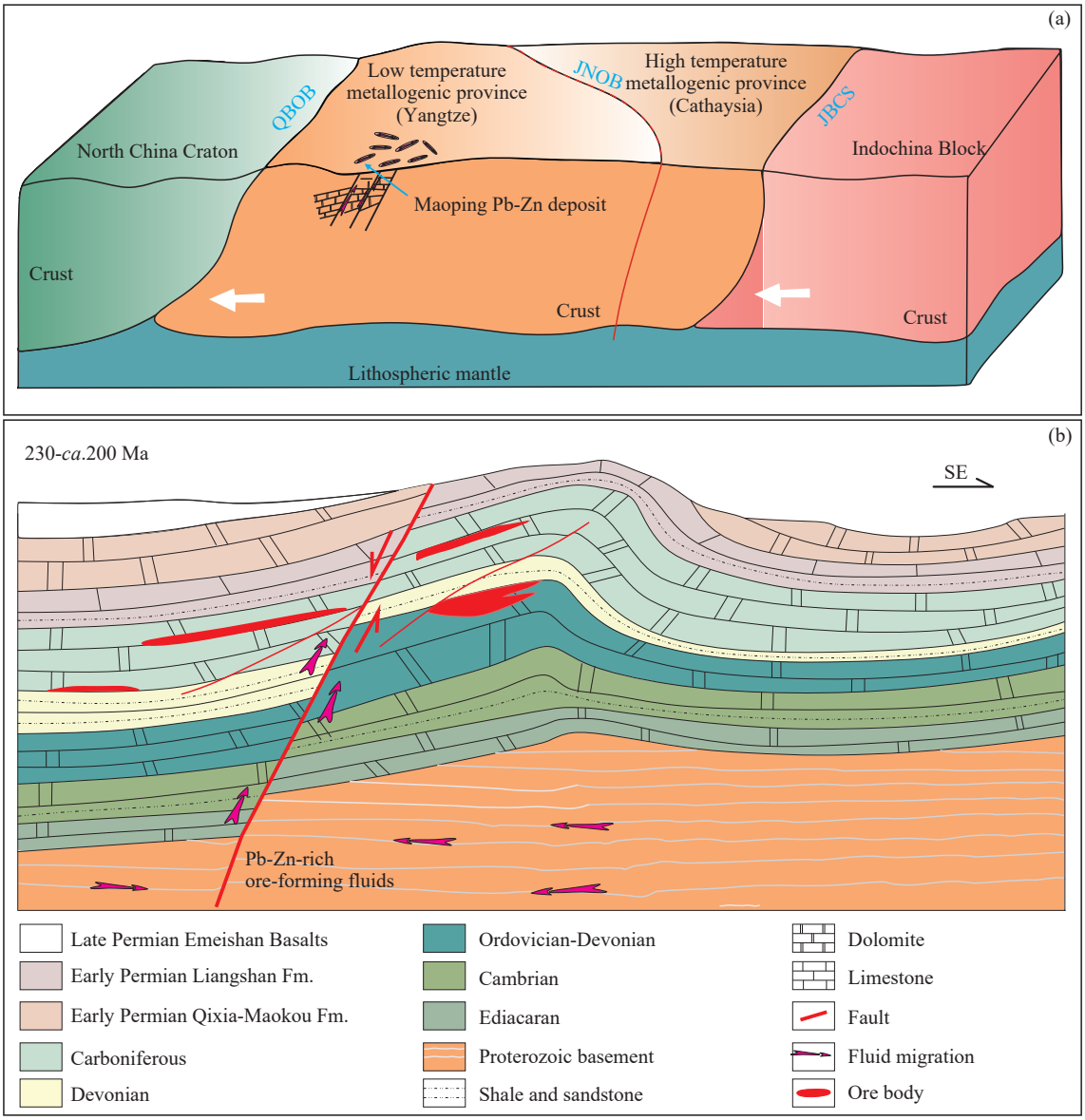

Fig. 17. (a) A regional metallogenic model was proposed for the formation of Pb-Zn deposits in the Upper Yangtze province (QBOB-Qinling-Dabie Orogenic Belt; JNOB-Jiangnan Orogenic Belt; JBCS-Jinshajiang-Bangxi-Chenxing Suture; modified from Hu RZ et al., 2017), (b) A coupled metallogenic model of fluid-structure-lithology assemblage was proposed for the formation of the Maoping deposit.

dissolved carbon species.

(v) The sulfur isotopes of the Maoping deposits indicate that the primary source is reduced sulfur from evaporite rocks in the surrounding stratigraphy. TSR is the major mechanism for generating reduced sulfur, while BSR may be responsible for the lower $\delta^{34}S$ values. The ore-forming metals (Pb) mainly derived from the Devonian-Carboniferous ore-bearing sedimentary rocks, and secondarily from the Precambrian basement rocks, with a possible minor contribution from Permian Emeishan basalts.

(vi) The Sr isotopes of hydrothermal carbonate minerals suggest that the ore-forming fluids originated from or passed through geological bodies rich in radiogenic Sr, most likely the Lower Cambrian black rock series. And the contribution of basement materials dominates, while the contribution of later stratigraphic materials becomes increasingly significant.

(vii) LA-ICPMS in-situ U-Pb dating of the main ore-forming stage calcite yielded an age of 214 ± 20 Ma, which is consistent with the overall mineralization age of 200-230 Ma in the region, thus representing the formation age of the Maoping deposit. This age reflects that its formation is the result of the combined action of the Emeishan mantle plume and the Indosinian orogeny.

(viii) The Maoping Pb-Zn deposit was formed during the Indosinian orogeny, and a coupled mineralization product of fluid-tectonic-rock combinations. It is like but not identical to the MVT deposits and belongs to the Upper Yangtze-type of Pb-Zn deposits.

CRediT authorship contribution statement

Ye He and Jia-Xi Zhou designed the conceptualization, presented the idea, and wrote the manuscript. Jia-Xi Zhou supervised the findings of this work. Bang-Tao Sun, Hai-Peng

Wang and Kai Luo contributed to the investigation, data curation, and visualization. Jia-Xi Zhou, Yan-Jun Li, Foteini Drakou and Saleh Ibrahim Bute polished the manuscript. Ye He, Jia-Xi Zhou, Yan-Jun Li, Foteini Drakou, and Kai Luo discussed the results and contributed to the final manuscript.

Declaration of competing interest

The authors declare no competing interests.

Acknowledgements

The Yiliang Chihong Co., LTD. were thanked for the help during the field work, and Drs. Jing Gu and Zhen-Zhong Xiang (Institute of Geochemistry, Chinese Academy of Sciences) were also thanked for their help of the experimental work. This study is financially supported by the National Natural Science Foundation of China (41872095, U1812402 and 42172082) and the Research Startup Project (YJRC4201804) of Yunnan University to J.-X. Zhou.

Supplementary data

Supplementary Tables. S1-S8 and Figures. S1-S2 to this article can be found online at doi: 10.31035/cg2024142.

References

Bai JH. 2013. Geochemistry and genesis of lead-zinc deposit in Jinshachang, Northeast Yunnan. Ph. D Dissertation. University of Chinese Academy of Sciences (in Chinese).

Bau M, Möller P. 1992. Rare earth element fractionation in metamorphogenic hydrothermal calcite, magnesite and siderite. Mineralogy and Petrology, 45(3), 231–246. doi: 10.1007/BF01163114.

Beaudoin G, Chiaradia M. 2016. Fluid mixing in orogenic gold deposits: Evidence from the H-O-Sr isotope composition of the val-d'Or vein field (Abitibi, Canada). Chemical Geology, 437, 7–18. doi: 10.1016/j.chemgeo.2016.05.009.

Brannon JC, Cole SC, Podosek FA, Ragan VM, Coveney RM Jr, Wallace MW, Bradley AJ. 1996. Th-Pb and U-Pb dating of ore-stage calcite and Paleozoic fluid flow. Science, 271(5248), 491–493. doi: 10.1126/science.271.5248.491.

Chaussidon M, Albarède F, Sheppard SMF. 1989. Sulphur isotope variations in the mantle from ion microprobe analyses of micro-sulphide inclusions. Earth and Planetary Science Letters, 92(2), 144–156. doi: 10.1016/0012-821X(89)90042-3.

Chen HS, Ran CY. 1992. Isotopic geochemistry of Kangdian earth axis copper deposit. Beijing: Geological Publishing House, 43–45 (in Chinese).

Chen X, Xue CJ. 2016. Origin of H_2S in uragen large-scale Zn-Pb mineralization, western Tien Shan: Bacteriogenic structure and S-isotopic constraints. Acta Petrologica Sinica, 32(5), 1301–1314 (in Chinese with English abstract).

Deng HL, Li CY, Tu GZ, Zhou YM, Wang CW. 2000. Strontium isotope geochemistry of the Lemachang independent silver ore deposit, northeastern Yunnan, China. Science in China Series D: Earth Sciences, 43(4), 337–346. doi: 10.1007/BF02959444.

Du LJ, Li B, Huang ZL, Zhou JX, Zou GF, Yan ZF. 2017. Carbon-oxygen isotopic geochemistry of the yangla Cu skarn deposit, SW China: Implications for the source and evolution of hydrothermal fluids. Ore Geology Reviews, 88, 809–821. doi: 10.1016/j.oregeorev.2017.01.026.

Faure G. 1977. Principles of isotope geology.

Gong H, Han R, Wu P, Chen G, Li L. 2021. Constraints of S-Pb-Sr isotope compositions and Rb-Sr isotopic age on the origin of the laoyingqing noncarbonate-hosted Pb-Zn deposit in the Kunyang Group, SW China. Geofluids, 8844312. Doi: 10.1155/2021/8844312.

Guan HM, Shi WM, Qin CL. 2020. The study of deposit genesis and metallogenic model of Zhangjiashan iron deposit, West Henan. Mineral Resources and Geology, 34(3), 401–407,414 (in Chinese with English abstract). doi: 10.19856/j.cnki.issn.1001-5663.2020.03.001.

Guo X. 2012. Mineralization and metallogenic pattern of lead-zinc deposits in Northeast Yunnan. Ph. D Dissertation. China University of Geosciences (Beijing) (in Chinese).

Han RS, Zou HJ, Hu B, Hu YZ, Xue CD. 2007. Fluid inclusion characteristics and ore-forming fluid source of Maoping Pb-Zn- (Ag, Ge) deposit, Yunnan. Acta Petrologica Sinica, 23, 2109–2118. (in English).

He Y, Zhou GM, Zhong H, Cheng Y, Yue ZP, Liu HS, Zhou JX. 2023. Enrichment characteristics and its geological significance of dispersed elements within sulfide minerals from the VI ore belt in the Maoping Pb-Zn deposit, Yunnan Province, China. Acta Petrologica Sinica, 39(10), 2985–3001 (in Chinese with English abstract). doi: 10.18654/1000-0569/2023.10.08.

He YF, Wu T, Huang ZL, Ye L, Deng P, Xiang ZZ. 2020. Genesis of the maoping carbonate-hosted Pb-Zn deposit, northeastern Yunnan Province, China: Evidences from geology and C-O-S-Pb isotopes. Acta Geochimica, 39(5), 782–796. doi: 10.1007/s11631-020-00424-4.

Hoefs J. 2004. Stable Isotope Geochemistry. Berlin, Heidelberg: Springer Berlin Heidelberg. Doi: 10.1007/978-3-662-05406-2.

Holland HD. 1979. The solubility and occurrence of non-ore minerals. Geochemistry of hydrothermal ore deposits, 461–508.

Hu RZ, Fu SL, Huang Y, Zhou MF, Fu SH, Zhao CH, Wang YJ, Bi XW, Xiao JF. 2017. The giant South China Mesozoic low-temperature metallogenic domain: Reviews and a new geodynamic model. Journal of Asian Earth Sciences, 137, 9–34. doi: 10.1016/j.jseaes.2016.10.016.

Huang ZL, Chen J, Han RS, Li WB, Liu CQ, Zhang ZL, Ma DY, Gao DR, Yang, HL. 2004. The geochemistry and genesis of the Huize super-large Pb-Zn deposit, and the relationship between the basalt and the Pb-Zn mineralization in Mount Emei. Beijing: Geological Publishing House, 187 (in Chinese).

Jiang YH, Li SR. 2005. Study on the isotope data tracing and isotopic chronology in the black–rock–series type Ni–Mo deposits in the Lower Cambrian in Hunan and Guizhou provinces. Mineral Rocks, 1, 62–66 (in Chinese with English abstract). doi: 10.19719/j.cnki.1001-6872.2005.01.012.

Jin XY, Zhao JX, Feng YX, Hofstra AH, Deng XD, Zhao XF, Li JW. 2021. Calcite U-Pb dating unravels the age and hydrothermal history of the giant Shuiyindong carlin-type gold deposit in the golden triangle, South China. Economic Geology, 116(6), 1253–1265. doi: 10.5382/econgeo.4870.

Jin ZG, Zhou JX, Huang ZL, Luo K, Gao JG, Peng S, Wang B, Chen XL. 2016. Ore genesis of the nayongzhi Pb-Zn deposit, Puding City, Guizhou Province, China: Evidences from S and in situ Pb isotopes. Acta Petrologica Sinica, 32(11), 3441–3455 (in Chinese with English abstract).

Leach DL, Bradley DC, Huston D, Pisarevsky SA, Taylor RD, Gardoll SJ. 2010. Sediment-hosted lead-zinc deposits in earth history. Economic Geology, 105(3), 593–625. doi: 10.2113/gsecongeo.105.3.593.

Leach DL, Sangster DF, Kelley KD, Large RR, Garven G, Allen CR, Gutzmer J, Walters S. 2005. Sediment-hosted lead-zinc deposits: A global perspective. One Hundredth Anniversary Volume: Society of Economic Geologists. Doi: 10.5382/av100.18.

Leach DL, Song YC. 2019. Chapter 9 sediment-hosted zinc-lead and

copper deposits in China. Mineral Deposits of China: Society of Economic Geologists, 325–409. Doi: 10.5382/sp.22.09.

Li LR, Li DL. 2016. Geological characteristics and prospecting significance of hexi ore section in Yiliang Maoping Lead-zinc deposit, Zhaotong. Western Resources, 2, 149–151 (in Chinese). doi: 10.16631/j.cnki.cn15-1331/p.2016.02.059.

Li WB, Huang ZL, Wang YX, Chen J, Han RS, Xu C, Guan T, Yin MD. 2004a. Age of the giant Huize Zn-Pb deposits determined by Sm-Nd datingof hydrothermal calcite. Geological Review, 50(2), 189–195 (in Chinese with English abstract). doi: 10.16509/j.georeview.2004.02.014.

Li WB, Huang ZL, Chen J, Han RS, Zhang ZL, Xu C. 2004b. Rb-Sr dating of mineral assemblage from the Huize giant Zn-Pb deposit, Yunnan provine. Acta Mineralogica Sinica, 24(2), 112–116 (in Chinese with English abstract). doi: 10.16461/j.cnki.1000-4734.2004.02.003.

Li WB, Huang ZL, Yin MD. 2007. Dating of the giant Huize Zn-Pb ore field of Yunnan Province, Southwest China: Constraints from the Sm-Nd system in hydrothermal calcite. Resource Geology, 57(1), 90–97. doi: 10.1111/j.1751-3928.2006.00007.x.

Liao KL, Lyu CL, Ma WF. 2020. The geological significance of Rb-Sr isotopic dating of sphalerite in Shanshulin Pb-Zn deposit in Guizhou. Mineral Resources and Geology, 34(2), 273–277 (in Chinese with English abstract). doi: 10.19856/j.cnki.issn.1001-5663.2020.02.013.

Lin ZY, Wang DH, Zhang CQ. 2010. Rb-Sr isotopic age of sphalerite from the Paoma lead-zinc deposit in Sichuan Province and its implications. Geology in China, 37(2), 488–494 (in Chinese with English abstract). doi: 10.3969/j.issn.1000-3657.2010.02.023.

Liu F. 2005. The metallogenic mechanism of the Huize large lead-zinc ore deposit and the occurrence of germanium, Yunnan Province, China. Ph. D Dissertation. Beijing: China University of Geosciences (in Chinese with English abstract).

Liu HC, Lin WD. 1999. Research on the regularity of lead-zinc-silver deposits in northeast Yunnan. Kunming: Yunnan University Press, 1–468 (in English).

Liu XK, Chen FC, Chang H, Gao JG, Wu P, Tan J. 2022. The mineralization of daxiao carbonate-hosted Pb-Zn deposit, northeast Yunnan Province, SW China: Constraints from Rb-Sr isotopic dating and H-O-S-Pb isotopes. Ore Geology Reviews, 147, 104956. doi: 10.1016/j.oregeorev.2022.104956.

Lottermoser BG. 1992. Rare earth elements and hydrothermal ore formation processes. Ore Geology Reviews, 7(1), 25–41. doi: 10.1016/0169-1368(92)90017-F.

Luo K, Cugerone A, Zhou MF, Zhou JX, Sun GT, Xu J, He KJ, Lu MD. 2022. Germanium enrichment in sphalerite with acicular and euhedral textures: An example from the Zhulingou carbonate-hosted Zn (-Ge) deposit, South China. Mineralium Deposita, 57(8), 1343–1365. doi: 10.1007/s00126-022-01112-4.

Luo K, Zhou JX, Feng YX, Uysal IT, Nguyen A, Zhao JX, Zhang JW. 2020a. In situ U-Pb dating of calcite from the South China antimony metallogenic belt. iScience, 23(10), 101575. doi: 10.1016/j.isci.2020.101575.

Luo K, Zhou JX, Huang ZL, Caulfield J, Zhao JX, Feng YX, Ouyang HG. 2020b. New insights into the evolution of Mississippi valley-type hydrothermal system: A case study of the wusihe Pb-Zn deposit, South China, using quartz in situ trace elements and sulfides in situ S-Pb isotopes. American Mineralogist, 105(1), 35–51. doi: 10.2138/am-2020-7021.

Luo K, Zhou JX, Huang ZL, Wang XC, Wilde SA, Zhou W, Tian LY. 2019. New insights into the origin of early Cambrian carbonate-hosted Pb-Zn deposits in South China: A case study of the maliping Pb-Zn deposit. Gondwana Research, 70, 88–103. doi: 10.1016/j.gr.2018.12.015.

Ma L, Chen HJ, Gan, KW, Xu KD, Xu XS, Wu GY, Ye Z, Liang X, Wu SH, Qiu YY, Zhang PL, Ge PP. 2004. Tectonic and marine oil and gas geology in southern China. Beijing: Geological Publishing House, 1–867 (in Chinese).

Mao JW, Zhou ZH, Feng CY, Wang YT, Zhang CQ, Peng HJ, Yu M. 2012. A preliminary discussion on the large-scale mineralization and its dynamic background of the Triassic in China. Geology of China, 39, 1437–1471 (in Chinese). doi: 10.3969/j.issn.1000-3657.2012.06.001.

Miao Y, Li W, Zhou JX, Luo K, Zhou Y, Chen SM, Fan ZY, Pan JR. 2023. Geology, geochemistry and genesis of the giant Maoping carbonate-hosted Pb-Zn-(Ag-Ge) deposit in northeastern Yunnan Province, SW China. Ore Geology Reviews, 161, 105648. doi: 10.1016/j.oregeorev.2023.105648.

Nakai S, Halliday AN, Kesler SE, Jones HD, Kyle JR, Lane TE. 1993. Rb-Sr dating of sphalerites from Mississippi Valley-type (MVT) ore deposits. Geochimica et Cosmochimica Acta, 57(2), 417–427. doi: 10.1016/0016-7037(93)90440-8.

O'Neil JR, Clayton RN, Mayeda TK. 1969. Oxygen isotope fractionation in divalent metal carbonates. 51(12), 5547–5558. doi: 10.1063/1.1671982.

Ren SL, Li YH, Zeng PS, Qiu WL, Fan CF, Hu GY. 2018. Effect of sulfate evaporate salt layer in mineralization of the Huize and maoping lead-zinc deposits in Yunnan: Evidence from sulfur isotope. Acta Geologica Sinica, 92(5), 1041–1055 (in Chinese). doi: 10.3969/j.issn.0001-5717.2018.05.010.

Seal RR. 2006. Sulfur isotope geochemistry of sulfide minerals. Reviews in Mineralogy and Geochemistry, 61(1), 633–677. doi: 10.2138/rmg.2006.61.12.

Shellnutt JG, Pham TT, Denyszyn SW, Yeh MW, Tran TA. 2020. Magmatic duration of the Emeishan large igneous province: Insight from northern Vietnam. Geology, 48(5), 457–461. doi: 10.1130/g47076.1.

Shentu LY, Han RS, Li B, Qiu WL. 2011. Study on the isotope geochemistry of the maoping Pb-Zn deposit, Zhaotong, Yunnan. Mineral Resources and Geology, 25(3), 211–216 (in Chinese). doi: 10.3969/j.issn.1001-5663.2011.03.008.

Shen ZW, Jin CH, Dai YP, Zhang Y, Zhang H. 2016. Mineralization age of the maoping Pb-Zn deposit in the northeastern Yunnan Province: Evidence from Rb-Sr isotopic dating of sphalerites. Geological Journal of China Universities, 22(2), 213–218 (in Chinese with English abstract). doi: 10.16108/j.issn1006-7493.2015196.

Shi H, Huang SJ, Shen LC, Zhang M. 2003. Strontium isotope composition of the Cambrian Luojiaguo section in Xiushan, Chongqing and its stratigraphic significance. Journal of Stratigraphy, 27(1), 71–76 (in Chinese with English abstract).

Tan SC, Zhou JX, Zhou MF, Ye L. 2019a. In-situ S and Pb isotope constraints on an evolving hydrothermal system, Tianbaoshan Pb-Zn-(Cu) deposit in South China. Ore Geology Reviews, 115, 103177. doi: 10.1016/j.oregeorev.2019.103177.

Tan SC, Zhou JX, Luo K, Xiang ZZ, He XH, Zhang YH. 2019b. The sources of ore-forming elements of the maoping large-scale Pb-Zn deposit, Yunnan Province: Constrains from in situ S and Pb isotopes. Acta Petrologica Sinica, 35(11), 3461–3476 (in Chinese with English abstract). doi: 10.18654/1000-0569/2019.11.13.

Tang YY, Bi XW, Zhou JX, Liang F, Qi YQ, Leng CB, Zhang XC, Zhang H. 2019. Rb-Sr isotopic age, S-Pb-Sr isotopic compositions and genesis of the Ca. 200 Ma Yunluheba Pb-Zn deposit in NW Guizhou Province, SW China. Journal of Asian Earth Sciences, 185, 104054. Doi: 10.1016/j.jseaes.2019.104054.

Taylor HP, Frechen J, Degens ET. 1967. Oxygen and carbon isotope studies of carbonatites from the Laacher See District, West Germany and the Alnö District, Sweden. Geochimica et Cosmochimica Acta, 31(3), 407–430. doi: 10.1016/0016-7037(67)90051-8.

Veizer J, Hoefs J. 1976. The nature of O^{18}/O^{16} and C^{13}/C^{12} secular trends in sedimentary carbonate rocks. Geochimica et Cosmochimica Acta,

40(11), 1387–1395. doi: 10.1016/0016-7037(76)90129-0.

Wang J, Zhang J, Zhang XJ, Liu WH, Zhong WB, Yang Q, Liu ZP. 2019. Rb-Sr chronology, stable isotopes and geological significance of sphalerite in Tianbaoshan deposit, Sichuan. Earth Science, 44(9), 3026–3041 (in Chinese).

Wang L, Han RS, Zhang Y, Zhou GM, Zhong H, Zuo JG, Deng P. 2022. Spatial structure of orebodies and prediction of deep orebodies of Maoping lead-zinc deposit, northeastern Yunnan Province. Mineral Deposits, 41(2), 207–224 (in Chinese with English abstract). doi: 10.16111/j.0258-7106.2022.02.001.

Wang L, Han R, Zhang Y, Li X, Wang L. 2023. Multi-layer metallogeny of the maoping carbonate-hosted Pb–Zn deposit, SW China: Constraints from C-O-S-Pb isotopes. Applied Geochemistry, 155, 105734. doi: 10.1016/j.apgeochem.2023.105734.

Wang LJ, Yu JH, Griffin WL, O'Reilly SY. 2012. Early crustal evolution in the western Yangtze Block: Evidence from U-Pb and Lu-Hf isotopes on detrital zircons from sedimentary rocks. Precambrian Research, 222, 368–385. doi: 10.1016/j.precamres.2011.08.001.

Wang T. 2018. Study on geology and genesis of the Maoping Lead-zinc deposit, Zhaotong, Yunnan, China. Ph. D Dissertation. Chengdu University of Technology (in Chinese with English abstract).

Wang WY, Gao JG, Nong YX, Chen XB. 2017. Rb-Sr isotopic geochronology and geochemical characteristics of S and Pb isotopes of the Lulu Pb-Zn deposit in Luquan, Yunnan Province. Geological Bulletin of China, 36(7), 1294–1304 (in Chinese with English abstract).

Wei AY, Xue CD, Xiang K, Li J, Liao C, Akhter QJ. 2015. The ore-forming process of the Maoping Pb-Zn deposit, northeastern Yunnan, China: Constraints from cathodoluminescence (CL) petrography of hydrothermal dolomite. Ore Geology Reviews, 70, 562–577. doi: 10.1016/j.oregeorev.2015.02.007.

Wu T, Huang ZL, He YF, Yang M, Fan HF, Wei C, Ye L, Hu YS, Xiang ZZ, Lai C. 2021. Metal source and ore-forming process of the maoping carbonate-hosted Pb-Zn deposit in Yunnan, SW China: Evidence from deposit geology and sphalerite Pb-Zn-Cd isotopes. Ore Geology Reviews, 135, 104214. doi: 10.1016/j.oregeorev.2021.104214.

Wu Y. 2013. The age and ore-forming process of MVT deposits in the boundary area of Sichuan-Yunnan-Guizhou provinces, southwest China. China University of Geosciences (Beijing) (in Chinese).

Xiang ZZ, Zhou JX, Luo K. 2020. New insights into the multi-layer metallogenesis of carbonated-hosted epigenetic Pb-Zn deposits: A case study of the maoping Pb-Zn deposit, South China. Ore Geology Reviews, 122, 103538. doi: 10.1016/j.oregeorev.2020.103538.

Xiong SF, Jiang SY, Chen ZH, Zhao JX, Ma Y, Zhang D, Duan ZP, Niu PP, Xu YM. 2022. A Mississippi Valley-type Zn-Pb mineralizing system in South China constrained by in situ U-Pb dating of carbonates and barite and in situ S-Sr-Pb isotopes. GSA Bulletin, 134(11-12), 2880–2890. doi: 10.1130/b36289.1.

Xu SH, Hu YZ, Cheng Y, Zhu JZ, Ping Y, Zhang QM, Pei ZX. 2023. Genetic relationship between the maoping Pb-Zn deposit and paleo-oil reservoir in the northern Yunnan-Guizhou depression: Evidence from bitumen trace elements and the in situ sulfur isotope of pyrite associated with bitumen. Frontiers in Earth Science, 10, 1109112. doi: 10.3389/feart.2022.1109112.

Yang B, Jin CH, Zhang Y, Ji PL, Guo Y, Wang ZZ. 2018. Ore deposit characteristics and metallogenic model of the maoping Pb-Zn deposit in Wumengshan mountainous area, Yunnan Province. Acta Geoscientica Sinica, 39(5), 593–605 (in Chinese). doi: 10.3975/cagsb.2018.073001.

Yang Q, Liu WH, Zhang J, Wang J, Zhang XJ. 2019. Formation of Pb-Zn deposits in the Sichuan-Yunnan-Guizhou triangle linked to the Youjiang foreland basin: Evidence from Rb-Sr age and in situ sulfur isotope analysis of the Maoping Pb-Zn deposit in northeastern Yunnan Province, southeast China. Ore Geology Reviews, 107, 780–800. doi: 10.1016/j.oregeorev.2019.03.022.

Yang Q, Zhang J. 2018. Rb-Sr dating of sphalerite and S isotope of sulfides from Maoping Pb-Zn deposit, Southwest China, and their geological implications. EGU General Assembly, 2880.

Yang Q. 2021. Study on Mineralization of lead-zinc deposits in Northeastern Yunnan and Northwestern Guizhou Province, China. Ph. D Dissertation. China University of Geosciences (in Chinese).

Yin MD, Li WB, Sun XW. 2009. Rb-Sr isotopic dating of sphalerite from the giant Huize Zn-Pb ore field, Yunnan Province, Southwestern China. Chinese Journal of Geochemistry, 28(1), 70–75. doi: 10.1007/s11631-009-0070-5.

Zartman RE, Doe BR. 1981. Plumbotectonics-the model. Tectonophysics, 75, 135–162. doi: 10.1016/0040-1951(81)90213-4.

Zhang CQ, Li XH, Yu JJ, Mao JW, Chen FK, Li HM. 2008. Rb-Sr dating of single sphalerites from the Daliangzi Pb-Zn deposit, Sichuan, and its geological significances. Geological Review, 54(4), 532–538 (in Chinese with English abstract). doi: 10.16509/j.georeview.2008.04.006.

Zhang CQ, Mao JW, Wu SP, Li HM, Liu F, Guo BJ, Gao DR. 2005. Distribution, characteristics and genesis of Mississippi Valley-Type lead-zinc deposits in Sichuan-Yunnan-Guizhou area. Mineral Deposits, 24(3), 336–348 (in Chinese). doi: 10.3969/j.issn.0258-7106.2005.03.013.

Zhang CQ, Wu Y, Hou L, Mao JW. 2015. Geodynamic setting of mineralization of Mississippi valley-type deposits in world-class Sichuan-Yunnan-Guizhou Zn-Pb triangle, Southwest China: Implications from age-dating studies in the past decade and the Sm-Nd age of Jinshachang deposit. Journal of Asian Earth Sciences, 103, 103–114. doi: 10.1016/j.jseaes.2014.08.013.

Zhang H, Meng CZ, Qi YQ, Tang YY, Jin XL, Chen X, Leng CB. 2016. Source of ore-forming materials in Yunluheba lead-zinc deposit, Northwest Guizhou Province: S and Pb isotope constraints. Journal of Mineralogy, 36(2), 271–276 (in Chinese). doi: 10.16461/j.cnki.1000-4734.

Zhang YX, Wu Y, Tian G, Shen L, Zhou YM, Dong WW, Zeng R, Yang XC, Zhang CQ. 2014. Mineralization age and the source of ore-forming material at lehong Pb-Zn deposit, Yunnan province: Constraints from Rb-Sr and S isotopes system. Acta Mineralogica Sinica, 34(3), 305–311 (in Chinese with English abstract). doi: 10.16461/j.cnki.1000-4734.2014.03.002.

Zhao WC, Zhu XY, Jiang BB, Zhao DS. 2023. Genesis of the carbonate-hosted zinc-lead deposits in the southwestern Yangtze craton, SW China: Insights from the maoping deposit. Journal of Geochemical Exploration, 250, 107234. doi: 10.1016/j.gexplo.2023.107234.

Zheng YF, Chen JF. 2000. Stable isotope geochemistry. Beijing: Science Press, 316 (in Chinese).

Zheng YF. 1990. Carbon-oxygen isotopic covariation in hydrothermal calcite during degassing of CO_2. Mineralium Deposita, 25(4), 246–250. doi: 10.1007/BF00198993.

Zheng YF. 2001. Theoretical modeling of stable isotope systems and its applications to geochemistry of hydrothermal ore deposits. Mineral Deposits, 20(1), 57–70,85 (in Chinese with English abstract).

Zhou JX, Huang ZL, Bao GP. 2013a. Geological and sulfur-lead-strontium isotopic studies of the shaojiwan Pb-Zn deposit, Southwest China: Implications for the origin of hydrothermal fluids. Journal of Geochemical Exploration, 128, 51–61. doi: 10.1016/j.gexplo.2013.01.007.

Zhou JX, Huang ZL, Lv ZC, Zhu XK, Gao JG, Mirnejad HS. 2014a. Geology, isotope geochemistry and ore genesis of the Shanshulin carbonate-hosted Pb-Zn deposit, Southwest China. Ore Geology Reviews, 63, 209–225. doi: 10.1016/j.oregeorev.2014.05.012.

Zhou JX, Huang ZL, Zhou GF, Li XB, Ding W, Bao GP. 2011. Trace

elements and rare earth elements of sulfide minerals in the Tianqiao Pb-Zn ore deposit, Guizhou Province, China. Acta Geologica Sinica - English Edition, 85(1), 189–199. doi: 10.1111/j.1755-6724.2011.00389.x.

Zhou JX, Huang ZL, Zhou MF, Zhu XK, Muchez P. 2014b. Zinc, sulfur and lead isotopic variations in carbonate-hosted Pb-Zn sulfide deposits, Southwest China. Ore Geology Reviews, 58, 41–54. doi: 10.1016/j.oregeorev.2013.10.009.

Zhou JX, Bai JH, Huang ZL, Zhu D, Yan ZF, Lv ZC. 2015. Geology, isotope geochemistry and geochronology of the Jinshachang carbonate-hosted Pb-Zn deposit, Southwest China. Journal of Asian Earth Sciences, 98, 272–284. doi: 10.1016/j.jseaes.2014.11.024.

Zhou JX, Gao JG, Chen D, Liu XK. 2013b. Ore genesis of the Tianbaoshan carbonate-hosted Pb-Zn deposit, southwest China: Constrained by C-H-O-S-Pb isotopic compositions Sm-Nd isotopic age. Journal of Asian Earth Sciences, 73, 39–47. doi: 10.1080/00206814.2013.782973.

Zhou JX, Huang ZL, Yan ZF. 2013c. The origin of the Maozu carbonate-hosted Pb-Zn deposit, Southwest China: Constrained by C-O-S-Pb isotopic compositions and Sm-Nd isotopic age. Journal of Asian Earth Sciences, 73, 39–47. doi: 10.1016/j.jseaes.2013.04.031.

Zhou JX, Huang ZL, Zhou GF, Zeng QS. 2012. C, O isotope and REE geochemistry of the hydrothermal calcites from the Tianqiao Pb-Zn ore deposit in NW Guizhou Province, China. Geotectonica et Metallogenia, 36(1), 93–101 (in Chinese with English abstract). doi: 10.16539/j.ddgzyckx.2012.01.009.

Zhou JX, Huang ZL, Zhou MF, Li X, Jin ZG. 2013d. Constraints of C-O-S-Pb isotope compositions and Rb-Sr isotopic age on the origin of the Tianqiao carbonate-hosted Pb-Zn deposit, SW China. Ore Geology Reviews, 53, 77–92. doi: 10.1016/j.oregeorev.2013.01.001.

Zhou JX, Xiang ZZ, Zhou MF, Feng YX, Luo K, Huang ZL, Wu T. 2018a. The giant Upper Yangtze Pb-Zn Province in SW China: Reviews, new advances and a new genetic model. Journal of Asian Earth Sciences, 154, 280–315. doi: 10.1016/j.jseaes.2017.12.032.

Zhou JX, Luo K, Wang XC, Wilde SA, Wu T, Huang ZL, Cui YL, Zhao JX. 2018b. Ore genesis of the Fule Pb-Zn deposit and its relationship with the Emeishan large igneous province: Evidence from mineralogy, bulk C-O-S and in situ S-Pb isotopes. Gondwana Research, 54, 161–179. doi: 10.1016/j.gr.2017.11.004.

Zhou MF, Malpas J, Song XY, Robinson PT, Sun M, Kennedy AK, Lesher CM, Keays RR. 2002. A temporal link between the Emeishan large igneous province (SW China) and the end-Guadalupian mass extinction. Earth and Planetary Science Letters, 196(3-4), 113–122. doi: 10.1016/S0012-821X(01)00608-2.

Zhu CW, Liao SL, Wang W, Zhang YX, Yang T, Fan HF, Wen HJ. 2018. Variations in Zn and S isotope chemistry of sedimentary sphalerite, Wusihe Zn-Pb deposit, Sichuan Province, China. Ore Geology Reviews, 95, 639–648. doi: 10.1016/j.oregeorev.2018.03.018.

Zou HJ, Han RS, Hu B, Liu H. 2004. New evidences of origin of metallogenic materials in the maoping pb-zn ore deposit, Zhaotong, Yunnan: R-factor analysis results of trace elements in ne-extending fractural tectonites. Geology and Exploration, 40(5), 43–48 (in Chinese with English abstract).